OPTICALLY-PROCESSED PROGRAMMABLE ASSEMBLIES OF NANOMATERIALS

A Dissertation

Presented to the Faculty of the Graduate School

of Cornell University

in Partial Fulfillment of the Requirements for the Degree of

Master of Science

by

Yuanze Xu

August 2020

© 2020 Yuanze Xu
ALL RIGHTS RESERVED

ABSTRACT

Concurrent advances in synthetic methods of nanomaterials have granted us with unprecedented control over chemical, physical and mechanical properties. From the perspective of bottom-up manufacturing, to incorporate these advances into real-world applications, there is an urgent need of assembly technique, which bridges the gap between synthesis of nanometer sized building blocks and millimeter sized devices. For example, in quantum dot based optoelectronic devices, traps need to be effectively suppressed during assembly to ensure a coherent charge transport. Optically-processed assembly techniques are promising emerging techniques since they intrinsically possess temporal and spatial control by changing the dosage of light source. Besides, these systems can often work in ambient conditions and the reaction time is usually short compared to thermal treatments, which makes it a facile and versatile technique. The processes are usually initiated with the excitation of electrons of the photosensitizers. The excited electrons then trigger reactions to connect building blocks. In a direct pathway building blocks are connected by photoresponsive ligands , while in a mediated pathway connections are triggered by photoinitiated release of chemicals.

This thesis will discuss two systems with different building blocks. In the first part, quantum dots are connected into two-dimensional superstructures at a fluid interface via photoinitiated release of chemical triggers. The superstructures and reaction kinetics are carefully characterized to explain the mechanisms to give insights for other systems with similar two-phase setup. In the second part, inorganic clusters are assembled into hierarchical porous structures. The formation mechanisms and corresponding conditions are identified with facile tunability of pore size distribution. The materials are incorporated into a separation column and a purification of drugs from carcinogenic impurities is successfully achieved.

BIOGRAPHICAL SKETCH

Yuanze Xu was born in China. After graduating from Suzhou High School, he joined a joint program between Nanjing Tech University and The University of Sheffield in 2014. Four years later, he was awarded the degree of Bachelor of Science with class one honours in chemistry. He started graduate studies at Cornell University in the fall of 2018 as a part of Hanrath group. He will graduate with a Master of Science degree in August 2020 and keep pursuing his academic achievements.

This thesis is dedicated to my parents for their love, support and encouragement.

ACKNOWLEDGEMENTS

The author wishes to thank and acknowledge Dr. Hanrath for his guidance and instruction; Dr. Fors for reviewing this thesis for public release; Jen-Yu Huang and Yingjie Gao for collaborative works and discussions.

This work is supported by National Science Foundation (NSF-CMMI 1635433). This work made use of the Cornell Center for Materials Research (CCMR) shared facilities, which are supported through the NSF MRSEC program (DMR-1719875). This work was performed, in part, at the Cornell NanoScale Facility (CNF), a member of the National Nanotechnology Coordinated Infrastructure (NNCI), which is supported by the National Science Foundation (Grant ECCS-1542081).

TABLE OF CONTENTS

LIST OF FIGURES

CHAPTER 1

NANOMATERIALS TO DEVICES

Abstract. Concurrent synthetic methodologies provide us with unprecedented functionality, uniformity and variety of basic building blocks. With bottom-up manufacturing approach, these building blocks can be integrated into assemblies with decent structural control. A complete fabrication route from atoms to devices is subsequently established, with structures below a few nanometers controlled by synthesis, mesoscale structures dominated by assembly technique and structures beyond that scale controlled by design. Challenging tasks that requires cooperative multifunctional system can now be tackled by programmable assemblies of materials with different properties. To explain and manipulate the interactions in the system of building blocks and fabrication media is essential for next generation devices.

1.1 Conventional Bottom-up Manufacturing

Everything around us is composed of combinations from the periodic table. The combinations is limited, however, if we consider the morphology of building blocks composed by these combination as a third axis to the periodic table, the choices are therefore unlimited. Concurrent advances in synthetic methods of building blocks have enabled unprecedented morphological control over size, shape and dimensionality. With the composition of things demonstrated, how they are made falls into two categries. One is called top-down approach, which seeks to start with a bulk material and then break it into small pieces using mechanical, chemical and other forms of energy. Another one is bottom-up approach, which seeks to build up small components into complex assemblies. Natural systems is a beautifully orchestrated bottom-up assembly spanning across different length scale, from angstrom to meters. Taking a creature as an example, the most basic building blocks are atoms or molecules (angstrom-sized). Then they form macromolecules such as proteins and DNA ($\sim nm$). The macromolecules can assemble into cells ($\sim \mu m$), which can conduct biological activities. Cells subsequently form tissues and organs ($\sim mm$). At this stage, the structures are complex enough that humans have spent decades to decipher. Finally, the creatures are made, packed with all these fascinating bottom-up assemblies.

Material scientists have been seeking methods to employ the natural hierarchy into material assemblies spanning accross different length scale. From angstrom to tens of nanometers, the structure of building blocks is controlled by synthetic methods. For example, when synthesizing nanocrystals with hot injection triggered hydrothermal nucleation, the particle size can be simply altered with temperature, and the size distribution can be controlled by different mechanisms such as Ostwald ripening, self-focusing and capping ligand steric effect. In addition, the morphology

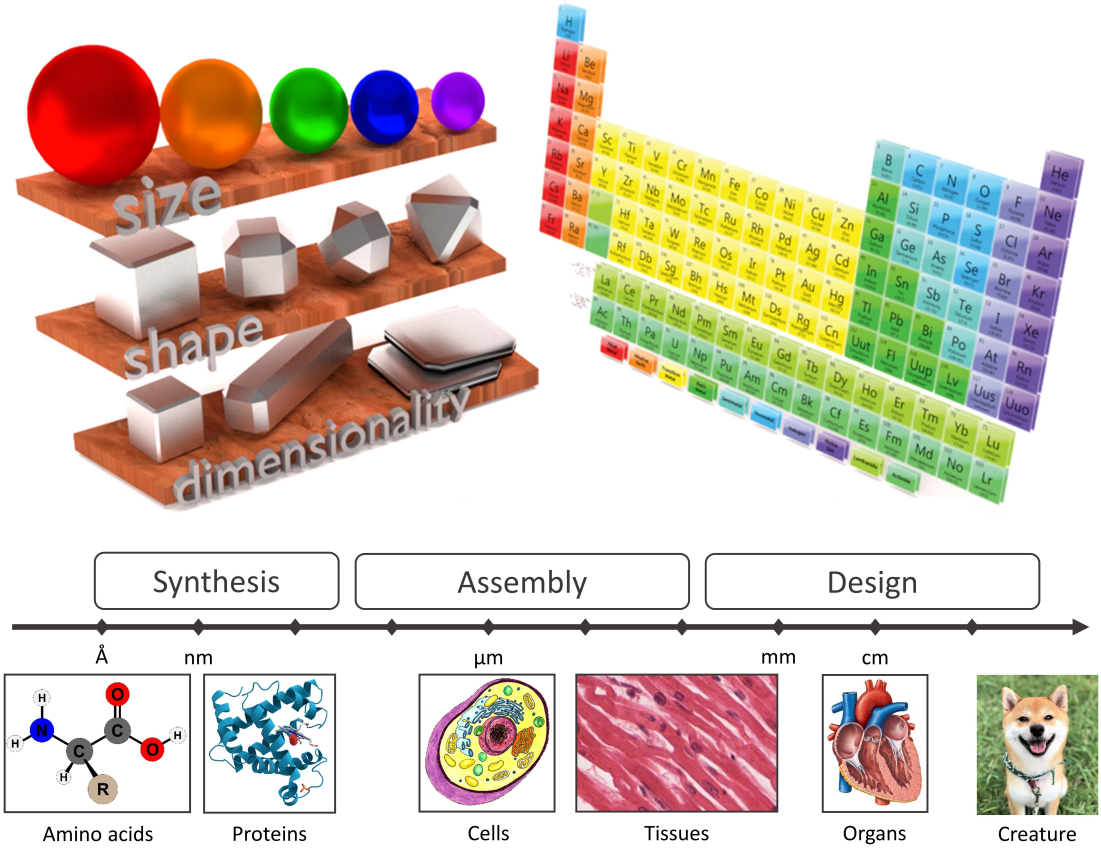

Figure 1.1: Conventional bottom-up manufacturing makes hierarchical structures spanning across whole length sacle as nature does.

can be altered by manipulating growth rates of different facets. Moving into larger length scale, sub-micron to tens of microns, these uniformly synthesized building blocks can be assembled with interactions between them, mostly by enthalpic, entropic and kinetic aspects. For exmaple, block-copolymers can self-assemble into micelle particles, rods or gyroids due to interaction with solvent. Finally, these assemblies are made into devices by specific designs such as arrays for computation, display and detectors, channels for separation devices and electrodes, and layered structure as scaffold.

There are multiple bottom-up approaches for fabrication of functional devices. Lithography techniques deposit 2D materials according to a spatially programmed

pattern, with a resolution down to a few nanometers. 3D printing is widely used in healthcare, energy, machine manufacturing and other industries for its facile, flexible and low-cost fabrication process of specific custom-designed parts. Thin film fabrication are broadly applied in surface modification of electrodes, catalysts, circuits, etc.

1.1.1 Lithography

Dip Pen Nanolithography (DPN)

Traditionally, DPN utilizes a cantilever tip to directly write patterns of materials, such as organic compounds, biological large molecules, nanoparticles, and polymers.[31] With a sharp scanning probe, such as the tip of atomic force microscope (AFM), droplets of chemicals are delivered to designated spots where the reaction happens to form desired nanostructures. The advantages of this technique include non-specific materials, high-resolution (sub-50 nm), ambient working conditions, *in-situ* imaging capability, and scalability.[30] In addition, a series of scanning probe technologies are developed based on DPN, including polymer pen lithography (PPL), scanning probe block copolymer lithography (SPBCL), and beam pen lithography (BPL).

Photolithography

Photolithogrpahy transfers a geometric pattern from a mask to photoresist on the substrate. A series of following steps, such as etching, developing and deposition, enables the ability to build another material according to the pattern. Currently,

this technique can create extremely small features, down to a few nanometers. A main shortcoming is that it requires a flat substrate to start with. Also, the operation environment are required to be extremely clean.

Electron Beam Lithography (EBL)

EBL uses a focused beam of electrons to draw patterns a responsive layer of resist on the substrate. The resist change solubility upon exposing to electron beam. The main advantage of EBL is that it directly draws a desired pattern, instead of using a mask.

Nanoimprint Lithography

Nanoimprint lithography converts patterns of self-assembled monolayers (SAMs) onto substrate surface by contact with the aid of the surface of a PDMS stamp. It differs from other lithography techniques for the usage of SAMs to form patterns

1.1.2 3D Printing

Powder Bed Fusion (PBF)

PBF uses a laser or an electron beam to melt and fuse materials in a build stage, where powders of precursors are fully packed. The pros of PBF include relatively low cost, visual models, ability to integrate technology into small scale, office sized machine, and large range of material options. However, there are still a few disadvantages include slow print speed, lack of structural properties in materials,

size limitations, and high power usage.

Direct Energy Deposition (DED)

In the DED process, the feedstock material, including metals, alloys, and steels, is pushed through a nozzle where it is melted by a focused heat source and successively added onto the build platform. Both the nozzle and heat source are mounted on a robotic arm. The whole system is often kept in protection atomsphere to avoid unwanted oxidation of the materials. DED is an ideal tool to repair and rebuild damaged components.The printing speed can be achieved up to 11 kg per hour. Other advantages include large scale fabrication, less materials waste, multi-component capabilities and high quality.

1.2 Manipulating Interactions between Building Blocks

Modern designs of bottom-up processing of nano building blocks fall into two categories. They are categorized base on whether the interactive part and functional part are integrated or separated.

1.2.1 Integrated Design

The first one involves an integrated engineering of the building blocks. Typically, an interactive layer of components, usually organic ligands, is coated onto functionalized cores, such as inorganic crystalline materials. These functionalized particles can be connected by different interactions of the coating layers. These interactions

include both weak interactions, such as Hydrogen bonding, and strong interactions, such as radical initiated C-C bonding, CLICK chemistry, and electrostatic forces. The strengths of this type of designs are mainly the integration of both functional parts and interactive parts. With most steps carried out in wet phase, this design can greatly reduce the number of components involved in each processing step, and subsequently increase the robustness and quality control of the product. For example, to fabricate a hierarchical porous superstructure, only solvent, ink, and photo initiator is needed. The weaknesses, however, are focused on the complexity of synthesis routes of such particles.

Covalent Bonded Networks

Hanrath *et al* have introduced a material design concept called Photoresponsive Ligand on Inorganic Core (PLIC). In this work, they functionalized oxozirconium clusters with methacrylate ligands, between which covalent bonds can form under UV light. PLIC design provides the ability to spatially program the macroscopic structures, while in the microscopic level, the structure is altered by using different PLIC cores as printing ink.

1.2.2 Synergistic Design

The other category is mainly a synergistic design of generalized particles and chemical trigger (CT). These chemical triggers either exchange or strip off the intrinsic ligands on the building blocks, change the solubility, and finally enable the formation of superstructures. Specifically, due to the stronger chelating effect, ethylenediamine can strip off oleate ligand to create a bare particle surface.

Oriented attachment between bare particles will be energetically favored to form superstructures, such as quantum dot solids. Photoacid generator (PAG) is another type of chemical trigger, which produces protons upon light excitation. The protons will facilitate the ligand detaching of oleate from particle surface, and then particles will be separated from wet phase due to solubility change. The advantage of this design is the high quality of the building blocks, in aspects of size distribution, stability, and morphology control. Since particles can be prepared through the most well-modified synthesis recipe without any post-treatments, any potential risk, such as etched surface, contaminated ligand shell, and aggregation, will be avoided. However, this deign often involves a reaction at the interface, so more factors should be taken in consideration, including spreading and intermingling of two phases, solvent effects, diffusion and solubility of reactants.

Direct Lithography

Photolithography finds its most significance in fabrication of integrated circuits. It utilizes a lithographed layer of photoresists, mostly polymer formulations, to create a spatial selectivity that other materials can be deposited with respect to. Within the exposed region of extreme ultraviolet light (EUV), photoresist is crosslinked. Unreacted photoresist is removed during developing step. The remaining patterned layer of photoresist serve as a barrier for plasma etching, such that plasma can selectively etch out those regions that are not protected by photoresist. After another developing step that removes the crosslinked photoresist layer, a patterned layer of materials is obtained. As introduced above, traditional photolithography needs a series of steps, including deposition of materials, developing and etching. If the materials is directly responsive to EUV, this process can be accelerated, and more robust since variances are less likely to be introduced in a simplified process

than a complicated one. Techniques which fall into this regime can be referred to as direct lithography.

Talapin *et al* have demonstrated a generalized direct lithography. A ligand called 1,2,3,4-thiatriazole-5-thiolate (TTT) is incorporated onto inorganic cores, including metals, semiconductors, oxides, magnetics and rare earth compositions. The inorganic cores are first deposited onto a substrate homogeneously. Then, with self-dissociation of TTT upon UV light exposure, the cores within exposure regions will become insoluble. Therefore, unreacted cores can be removed by solvent, leaving a lithographed layer of materials. They have also showed that the resolution is comparable with state-of-the-art techniques without compromising optic and electronic properties. This work is an important step in wet processed particle assemblies for its versatility and simple design.

CHAPTER 2

QUANTUM DOTS TO SUPERSTRUCTURES

Abstract. Ever since its discovery, quantum dots, with a tunable band structure, are believed to have prospects in optoelectronic devices. Recent advances in synthetic methodology and assembly technique have opened a gate to control material properties by design. Here, I present a facile two-phase fabrication technique of 2D superstructures of quantum dots. A chemical trigger is released with dissociation of protective groups, which stericly hinder its reactivity. Since the release is induced by photoinitiated electron transfer from quantum dots to protective groups, the concentration of chemical trigger can be temporally and spatially controlled by the light source dosage. Then I demonstrate that the optical and structural properties of the superstructures are a function of exposure time. The decomposition of semi-stable CdSe quantum dots are also investigated to help create a hybrid structure of two type of quantum dots, where small unstable dots decompose to form bridges between large stable dots. With this technique, a 2D patterned layer of CdSe are fabricated. Futhermore, a 3D structure can be obtained by additive manufacturing of these layers.

2.1 Introduction

Colloidal quantum dots (CQDs) is a promising platform for low-cost, scalable, flexible and programmable device manufacturing.[25] Potential applications include light-emitting diodes, photovoltaics and photodetectors. Unlike bulk semiconductors, whose electronic structures are solely determined by composition, the properties of individual QDs can also be tailored by the size, shape and surface ligands. This unique nature of CQDs offers an additional freedom to engineer the band structure by synthesis and the interaction between QDs by surface functionalization.

The large surface area of QDs is both a opportunity and a challenge. The surface trap states can severly hinder charge transport and luminescence. If properly engineered, however, with passivated traps and strong coupling between neighboring QDs, unprecedented device performance can be achieved.

2.1.1 Colloidal Quantum Dots

Quantum dots are often made with II-VI, III-V and IV-VI semiconductors.[45, 37] The synthesis can be precisely controlled to nearly single atomic layer. The surfaces of QDs are often coated with a layer of surfactant ligands, which keep CQDs stable from precipitation. By spreading and drying of CQDs, thin film of QDs can be coated or printed onto desired substrates.

Quantum Confinement

In semiconductor materials, the band gap energy is the minimum energy required to excite an electron from valence band to conduction band, corresponding to the peak with the largest wavelength in absorption spectrum. When any of the three dimensions of a semiconductor is smaller than the Bohr radius, which is the radii of an exciton generated in that material, the band gap is widened due to the confinement of exciton.[14, 8] This means as the particle gets smaller, the absorption and emission spectra is red-shifted. The band structures are different for nanoplatelets, nanowires and nanocrystals, since they are confined in 1D, 2D and 3D respectively. When a particle has all three dimensions smaller than the bohr radius, its energy level becomes discrete. [1]

Lead chalcogenide QDs are promising phosphores for bioimaging applications, since they often show absorption and emission peak at the near-infrared (NIR) region. Light within this region are more penetrable through animal tissues. To mitigate the toxicity of lead based particles, a protection layer, which is often composed by surface ligands or crystalline shells, is needed to separate lead cores and the environment. The first excitonic peak of Cadmium chalcogenide QDs can be tuned across the whole visible spectrum. Therefore, they are potential photocatalyst for visible light energy harvesting. Similarly, a crystalline shell, such as oxide materials, are often applied to prevent the core from oxidation and suppress surface traps.

Synthesis

Unlike lithographic techniques developed in integrated circuits industry, which, as a top-down approach, aggressively break large single crystals into small features,

synthesis of quantum dots utilizes a bottom-up approach that nucleates precursors in a wet phase. Solution processed QDs substaintially reduces the cost of device manufacturing and relieves the restrictions on light source, temperature, energy and compatibility. A systematic library of synthetic methodology of QDs has been developed ever since 1993.[36] Synthesis of colloidal QDs often involves nucleation of precursors, such as metal salts or organometallic compounds. The procedure can be described as a sequence of injection triggered nucleation, growth of crystal cores, separation of NCs, and post-treatment. To get monodispersed QDs solutions, multiple mechanisms are used. Ostwald ripening, as first described by Wilhelm Ostwald at 1896, is a thermodynamically driven process where larger particles grow at the expense of small particles. Since atoms at QD surface are more energetically unstable, smaller QDs are more likely to dissolve and redeposit onto larger ones. The synthesis of NCs usually takes place in the presence of organic surfactants, called 'ligands'. These organic compounds dynamically attach to QD surface and help prevent agglomeration. Besides, ligands can alter the properties of QDs. For example, ligands can create or eliminate surface trap states of semiconductor NCs. Charged ligands will form a ζ potential shell on QD surface, which gives electrophoretic mobility. DNA based ligands will have hydrogen bonding with each other, and thus directing the self-assembly of QDs.

2.1.2 Oriented Attachment of Faceted Quantum Dots

With photo-initiated radical polymerization, quantum dot (QD) superlattice (SL) can be fabricated with high level structural control. However, the unique semiconductor properties may not be conserved in this design, because the organic insulators betIen QDs will hinder charge transport, and quench excited electrons.

To obtain conserved optic and electronic properties, an alternative method to connect QDs has been proposed. With a chemical trigger, ligands on QD surface can be stripped off, and then fusion of neighboring QDs will be energetically favored to reduce high surface energy. To be specific, I use ethylenediamine (EDA) to trigger L-type ligand stripping. As described in other related works, EDA is added to the system via injection. In this case, the local concentration of EDA is completely determined by diffusion. The inevitable inhomogeneity caused by random diffusion hinders the performance of the devices.

Faceted Quantum Dots

It has been known that the atomic structures exposed on facets of a crystal give rise to specific chemical and physical properties. Therefore, over the last two decades, how to control the shape of QDs to be a polyhedron with desired facets has been intensively studied. The growth of the crystal is different for each facet due to the innate structural anisotropy. With anisotropic lattice, nanorods can be synthesized with a faster growth rate in one of the three crystal axes.[40] With lattice isotropic in all axes, polyhedrons of QDs with different perferred facets can be synthesized. Under high temperature, since ligands bond weakly to surface, the growth of facets with higher surface energy are preferred. Under relatively low temperature, strongly bonded ligands slows down the growth and favor lower energy facets.[32] Specifically for PbSe QD synthesis, the interactions between different facets and ligands are critical in tuning the shape of QDs.[10] For uncapped PbSe QDs, the {110} facets have higher surface energy than the {100} facets. When the surface ligand, oleic acid, is in low concentration, the {110} facets are more passivated to have a lower energy than {100} facets, resulting in an octahedron shaped QD. However, when oleic acid concentration is high, the {100} facets are

well-passivated, leading to a cubic structure.[6]

QD Superlattice via Oriented Attachment

The synthesis of faceted QDs with well-defined shape and narrow size distribution is essential in the formation of QD superlattices (SLs), which is an secondary ordered structure beyond the atomic lattice of QDs. In ordered arrays of QDs, the overall structure is equivalent to a lattice structure where the atoms are replaced with QDs. In SLs, neighboring QDs are connected via oriented attachments, which means the bondings are epitaxial such that atomic interactions fuse facets and the atmoic structure is coherent in long range to form mesocrystals.

It was reported in 2010 that PbS QDs can assemble into large 2D nanosheets via oriented attachments while still conserving quantum confinement in one dimension, but the detailed structure of the nanosheet was not clearly indicated.[43] In 2013, Vanmeakelbergh group systematically investigated superlattice formation with PbSe QDs via chemical and thermal treatment.[15] They showed that neighboring QDs are connected with atomic coherence and the superlattice structure vary from 1D wires to 2D hexatic and cubic assemblies. The same group demonstrated a detailed mechanistic study on the alignment process of individual QD at fluid interface.[20] It was revealed that QDs first move to specific positions of a hexatic assembly, then rotate to let {100} facet point upward, and finally as ligand is removed, the QDs fuse into cubic mesocrystals. Ethylene glycol is a dense and viscous liquid, and is a desired platform for CQDs assembly since solution of OA-capped QDs, presumably non-polar solvents, can easily spread on top of it. At the surface of ethylene glycol, the surface ligands of QDs are in a dynamic adsorption and desorption equilibrium, and therefore they will drop from the surface eventually if the subphase was not pre-formulated with oleic acid as solute. Although the

bare surfaces of QDs can then fuse by epitaxial bonding, this process often takes a few hours. An alternative way is to add a chemical to strip off the ligand and trigger the epitaxial connection. Owen *et al* have presented that the surface ligands of II-VI semiconductor QDs can be stripped off by a collection of chemical trigger.[2] Among these chemical triggers, diamines are often preferred for higher solubility in ethylene glycol and stronger stripping reactivity due to chelation. Although removal of ligands may introduce additional surface trap states, they can be passivated by post-treatment with halogen or hydroxy.[23, 7, 55] With the injection of ethylene diamine to trigger transformation of QD SLs from unconnected hexatic assembly to fused cubic solids, Hanrath group showed electronically coupled QDs over a square micrometer.[52] With similar chemical treatments, transistors with average two-terminal electron mobilities of 13 $cm^2V^{-1}s^{-1}$ and contactless mobility of 24 $cm^2V^{-1}s^{-1}$ were achieved.[4]

Advanced characterization equippments were used to study the interesting and intriguing formation mechanisms of these QD SLs. The Hanrath reported a phase transition mechanism that the SL transformations from hexatic to cubic happen simultaneously at different nucleation locations, and the inevitable shrinkage due to ligand removal can create grain boundaries which hinder the optoelectronic performance.[50] In addition to connections via {100} facets which result in a cubic superlattice, PbSe QDs can also be fused via different facets, the formation mechanism of different topologies were examined later from the aspects of enthalpy, entropy and kinetics.[51] Electron microscope pixel array detector (EMPAD), which generates a 2D array of 2D electron diffraction patterns at a resolution of 2 nm, offers unprecedented structural details to the orientation of each individual QD. A workflow with this powerful tool has been established, in which the misalignment of atomic lattice between neighboring QDs and mismatch of superlattices

can be statistically calculated via computer algorithms.[12] Besides QD orientational change on subphase, the coupled dynamics of top-phase solvent spreading and drying has been studies by *In-situ* grazing incident small-angle X-ray scattering (GISAXS).[3] They showed that the a monolayer of CQDs will spread even faster before the top-phase solvent periphery to form a pre-assembled layer before solvent is dry.

2.2 Temporal & Spatial Chemical Trigger (CT) Release

As in other related works, chemical trigger (CT) are always added by injection. HoIver, after injected into system, CT concentration is completely dominated by diffusion. Such lack of control greatly hinder the progress in basic mechanistic insights, finely modified assembly process, and scaling up into device making.

To obtain mechanistic insights, researchers often fabricate superlattices under different conditions and take electron microscope images to analyze how the microscopic structures can be related to the conditions used. The electron microscope reveals detailed structures with length scale of sub-micron, but the inhomogeneity caused by random diffusion of CT is so dramatic that microscopic structures can be completely different even in the same sample. Therefore, large replications of experiments are often needed to average out such uncertainty, which greatly slows the progress in this field. A guaranteed homogeneous reproducible concentration profile is crucial because it helps produce reliable data.

When making devices with chemical treatment, the reproducibility is of great importance. For example, in QD-based photodetector arrays, differences betIen how individual detector respond to the same light causes the noise of the overall photodetector. This performance is closely related to the coupling betIen neighboring

QDs, which is a result of specific chemical treatment. Therefore, a reproducible chemical treatment is so important for device fabrication that Ill-controlled CT release is urgently needed.

Furthermore, as I can envision, the ability to introduce CT via a controlled way will give accessibility to emerging assembly techniques. For example, as described in previous section, K. Whitham proposed a phase transition where the superstructure convert from hexatic superlattice to square connected QD solid by reduction in interparticle distance. The phase transition will cause cracking defect because as the surface ligand is removed, there will be an inevitable shrinkage of superlattice. The cracking caused by the shrinkage will negatively affect the optoelectronic performance, since charge transport will be interrupted by these defects. The ability to create a CT concentration gradient possess the potential to modify the phase transition, such that the contraction of QD superlattice only happen through one direction, and the interparticle space will be pushed to the opposite direction. This will greatly increase the grain size of QD solid.

With the need of controlled CT concentration profile exist in mechanistic study, device fabrication and tools for advanced processing, switching from brute force to clever chemistry is required. Since diffusion is random and can hardly be controlled, the goal will be to minimize diffusion effect in the system. Although temperature ramping, which means to trigger reaction with heat, can be homogeneously carried out, the processing time will be extended as an expense of homogeneous temperature profile. Photoinduced reactions can serve as a fast alternative to temperature ramping, where the reaction rate is related the to number of photons received by the reactants. HoIver, the choices of inorganic materials that can be processed with light is limited. Specifically, to fabricate QD superstructures, I keep the chemical treatment step, but the addition of CT is engineered to be photoresponsive in-

stead. In this way, the diffusion of CT and reaction of CT with QD is separated to minimize the effect of diffusion.

2.2.1 Photoinduced Electron Transfer (PET)

Generally, photoinduced electron transfer (PET) moves an electron to a higher energy level at the expense of incoming photon energy. When a photosensitizer absorbs a photon, one electron in ground state will first be promoted to excited state, leaving a hole in the ground state. In an oxidative quenching, the excited electron will be transferred to the acceptor. In a reductive quenching, the hole will be transferred to the donor. Since it is a catalytic cycle, the real donor or acceptor will then compensate for the remaining hole or electron respectively. In the oxidative quenching, there are two ways of transferring electrons from photosensitizers to acceptors. One is direct electron transfer, where the excited electron is directly transferred to acceptor right after photoexcitation. While in the other one, mediated electron transfer, the hole in ground state will first be transferred out to real donor before the excited electron is transferred.

Metal complexes are often used as catalytic photosensitizers in these PET cycles. The metal center atoms can absorb light and conduct metal-to-ligand charge transfer (MLCT) to facilitate the subsequent PET. Due to chemical stability, high yield and visible light absorption, ruthenium complex is probably the most ubiquitous one. HoIver, there are some concerns about these complexes, including high price and heavy metal waste. Recently, quantum dots have emerged to be an alternative for these metal complexes. Different from MLCT in metal complexes, the unique band structure of quantum dots enables generation of excitons, which are pairs of electrons and holes, in valence band and conduction band respectively. The

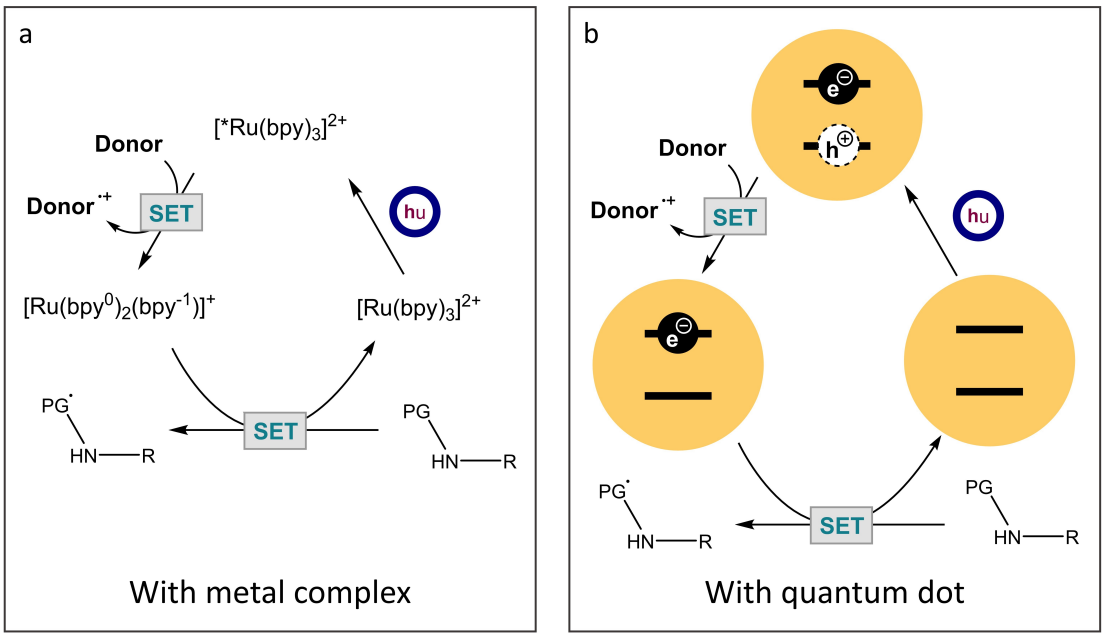

Figure 2.1: PET catalytic cycles via a) Ru complex or b) QD.

electrons, when promoted to conduction band, have similar catalytic property as charges created by MLCT. Besides, due to quantum confinement, the band structure of QD is tunable by its size, which, thanks to concurrent synthetic advances, can be easily altered during preparation of QDs. This flexibility is a poIrful tool in engineering the selectivity and reactivity towards different compounds. As shown in 2.1, the catalytic cycle via a ruthenium complex or a QD is similar, both include photoexcitation, single electron transfer (SET) from donor to catalyst, and SET from catalyst to acceptor.

2.2.2 Quantum Dot Catalyzed Amine Release

Since QDs are less likely to be engineered to be photoresponsive, photo-responsive CT is considered a promising way to control temporal and spatial profile of CT concentration. Ideally, the compound will be inert and become reactive upon light

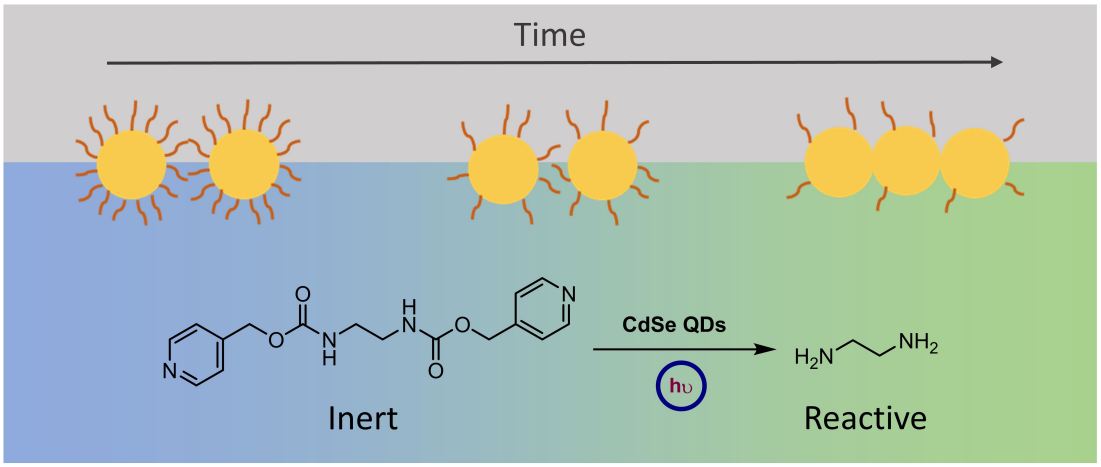

Figure 2.2: Optically release CT and control QD superlattice structure with exposure time.

exposure (2.2). In this way, the CT can be homogeneously spread into the system before light goes in, which separates the diffusion of CT and its reaction with QDs. With diffusion minimized, the spatial distribution and transient concentration can be controlled only by number of photons projected in designated areas. In this work I focus on II-VI QDs. As reported previously by OIn et al, amines can strip off surface ligands of II-VI QD, leaving a bare QD surface. The QD will fuse with neighboring ones to minimize surface energy, resulting a organic-free QD solid. I specifically chose ethylenediamine (EDA) as the CT, because of Ill-established reaction kinetics of EDA with oleic acid (OA) capped II-VI QDs. I capped the reactive Nitrogen site with a bulky protective group, which will stericly block the reactivity of EDA. This protective group, after being reduced with excited electrons, will self-dissociate as radicals, leaving a carboxylate, which will also spontaneously detach. Therefore, the EDA can be successfully released with PET to protective groups, as proposed in 2.3.

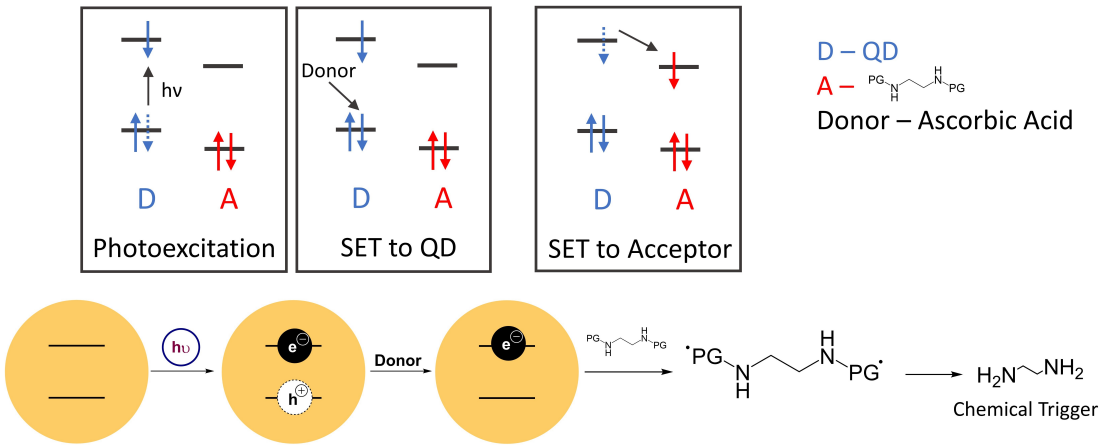

Figure 2.3: EDA release pathway via QD catalyzed protective group dissociation.

2.3 Patterning at Fluid Interface

Light controlled processing techniques find their applications in 3D printing, photolithography, and many other emerging fields. As a proof of concept, here I demonstrate the successful reaction with a 2-dimensional patterning at a fluid interface. This patterning technique can be vieId as a slice of a 3D object, or a photolithographic layer. Therefore, it falls Ill into the intersection of additive manufacturing and photolithography.

2.3.1 Two-phase Mechanism

Upon light exposure, an electron in QD is first excited to conduction band, leaving a hole in valence band. The hole is then transferred out to ascorbic acid. The excited electron can be transferred to protective group. The protective group, once received an electron, will undergo a spontaneous dissociation reaction, folloId by the detach of carboxylate groups. The dissociated radical is quenched with ascorbic acid. After each cycle, an ascorbic acid is oxidized. After this series of

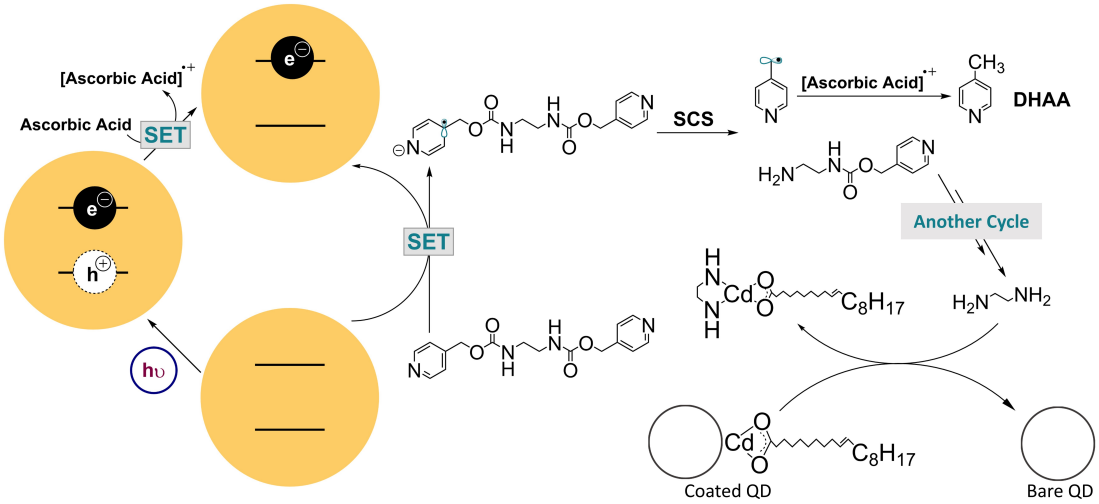

Figure 2.4: Proposed synergistic mechanism of EDA release via PET and subsequent ligand stripping.

reactions, EDA becomes reactive, and serves as ligand stripping reagent to remove the surface oleate of QD to convert it from coated to bare. Finally, neighboring bare QDs will attach with each other, driven by reduced surface energy.

This self-catalyzed synergistic reaction mechanism has advantages over metal complex catalyzed mechanisms. The EDA is released on QD surface, where the protective groups receive excited electrons. In addition, the following ligand stripping, which has a faster reaction rate, is also happening at QD surface. Therefore, the EDA will be consumed right after it is generated, greatly minimizing the diffusion effect. If EDA can be completely consumed on QD surface, the theoretical resolution will depend on individual QD size or light source, whichever is larger. The EDA-precursor can be viewed as a special CT, such that it only reacts with photoexcited QDs. Metal complexes dissolve in bulk with EDA-precursor, and the resolution will therefore suffered from diffusion, since the EDA has to randomly diffuse to touch QD surface to trigger ligand stripping reaction.

In order to successfully facilitate the electron transfer from QD to EDA-precursor and catalyze the reaction, the conduction band energy should be raised above that

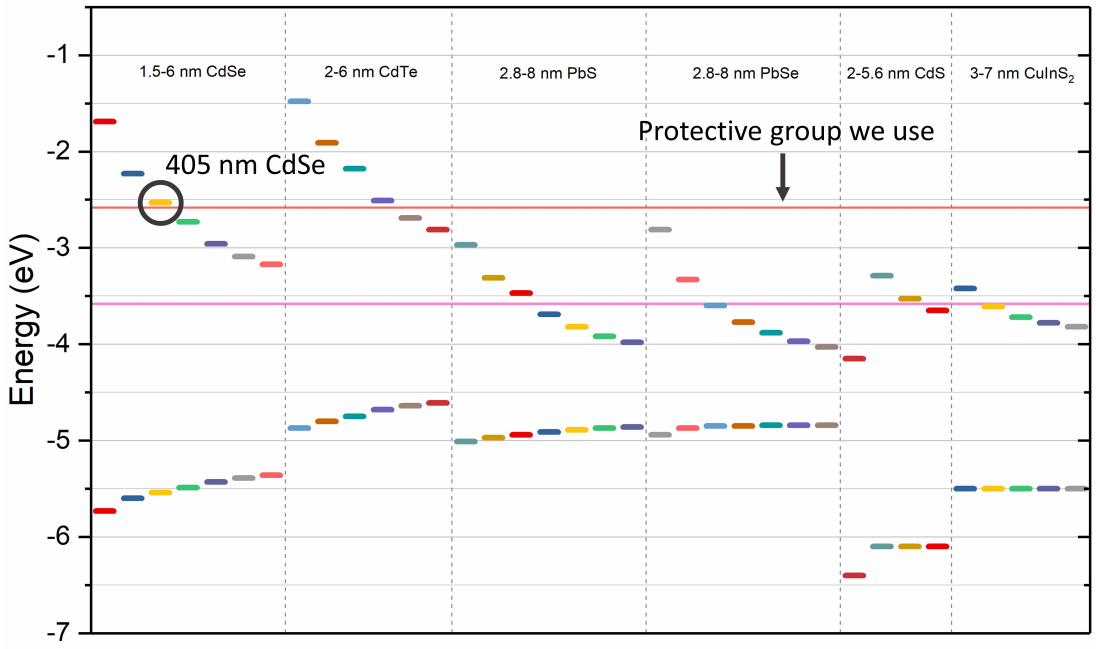

Figure 2.5: Band structure of QD with different size and composition, compared to reduction potential of protective groups.

of protective group. The band structure of QD with different materials and sizes is compared with the reductive potential of the protective group (2.5). Finally, I chose the 1.6 nm CdSe QD with first absorption peak at 405 nm. Detailed synthesis routes can be found in methods section.

2.3.2 Standard Operation Procedure

To incorporate such mechanism into the fabrication system, I employed a two-phase setup, as shown in 2.6 a.

As for the standard operation procedures (SOP) of the patterning, firstly, 1 mL of an ethylene glycol solution of EDA-precursor and ascorbic acid, 6.0 mg/mL and 14.0 mg/mL respectively, is injected into a 15x15x15 mm Teflon Ill. The ink is then injection on top of the subphase, and the solvent is evaporated to achieve a

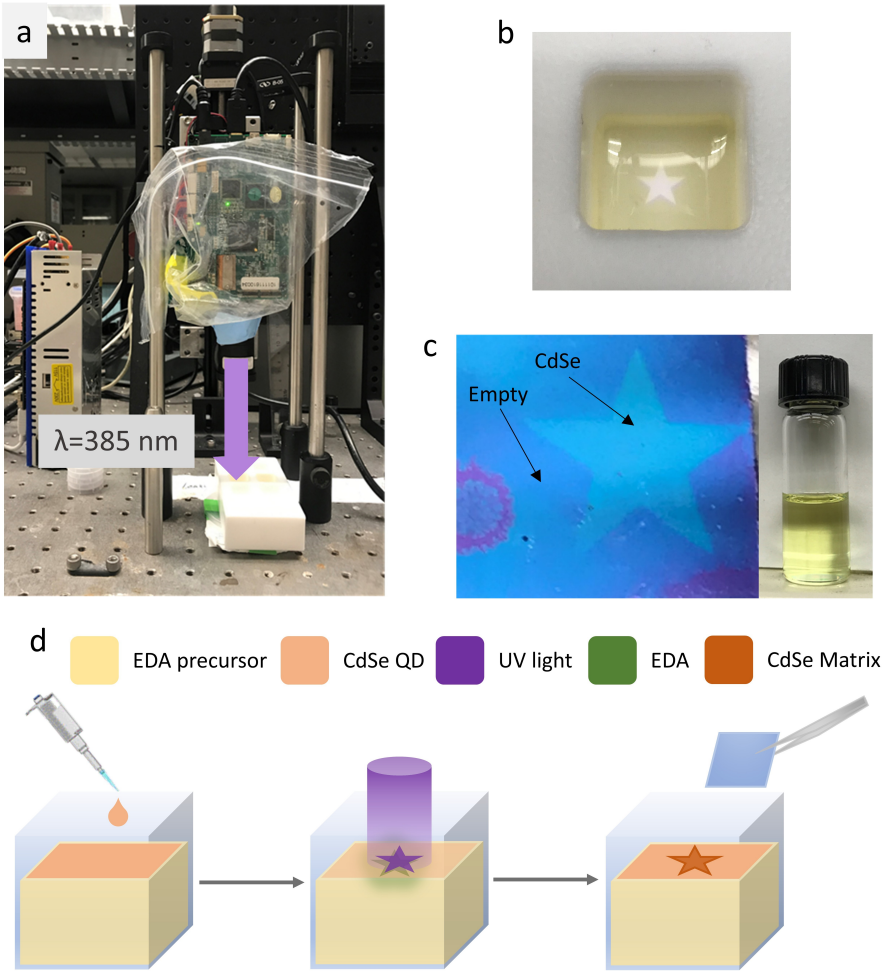

Figure 2.6: Two-phase setup for digital light processing: a) UV-light projector, b) UV pattern at fluid interface, c) example of a printed pattern, d) standard operation procedure (SOP).

pre-assembled layer. The choice of solvent, volume, and concentration of ink is determined by the desired pattern thickness. Typically, to achieve a 100 nm thick layer, I use 15 μL of 4.0 mg/mL hexane solution. The evaporation step takes about 5 minutes, with a glass slide covering the Teflon Ill. Once the pre-assembled layer is formed, a shaped UV light is projected onto the layer to trigger the reaction. The curing step takes a few minutes. Finally, the layer is transferred to a desired substrate for further use. Desired substrates include Si wafer (for visualization and thickness/roughness test), quartz slide (for optical measurements, such as UV-Vis

absorption and Photoluminescence), undoped Si wafer (for FTIR), TEM grid (for electron microscopy), and pre-printed FET wafer (for conductivity test).

Setup

Specifically, for patterning and mechanical property study, the film is transferred to a piece of wafer. Silica wafer functionalized with hexamethyldisilazane (HMDS), which has higher affinity to CdSe QDs and larger contact angle with EG, has been used. The functionalization step was done by immerse Si wafer in hot HDMS solution for hours. Besides the substrate treatment, a series of post-treatment is required after contacting pick up of QD film from the interface. After lifted with wafer, the film is immediately rinsed with methanol to remove remaining EG attached to film. I observed that remaining EG can tear the film apart within 1 minute. The wafer is then put in a vacuum chamber for 5 min to allow the excess methanol to evaporate. The remaining methanol droplets on the film, if not removed quickly, will form defects. Then the wafer undergoes several times of toluene rinse to remove the unreacted QDs (Figure 2.6a). The patterns become clearer, and the average thickness of the film is reduced.

Defects

Different types of defects are identified, together with proposed mechanisms for each of them. Cracks is formed by the interaction with walls of Teflon Ill. While the top phase is evaporating, strong tension can form if the pre-assembled layer touches the walls. After ligands betIen QDs are stripped off, an inevitable shrinkage of the top layer will increase the tension and finally tear the film into pieces. To avoid this, the spreading and drying profile should be carefully controlled, such that

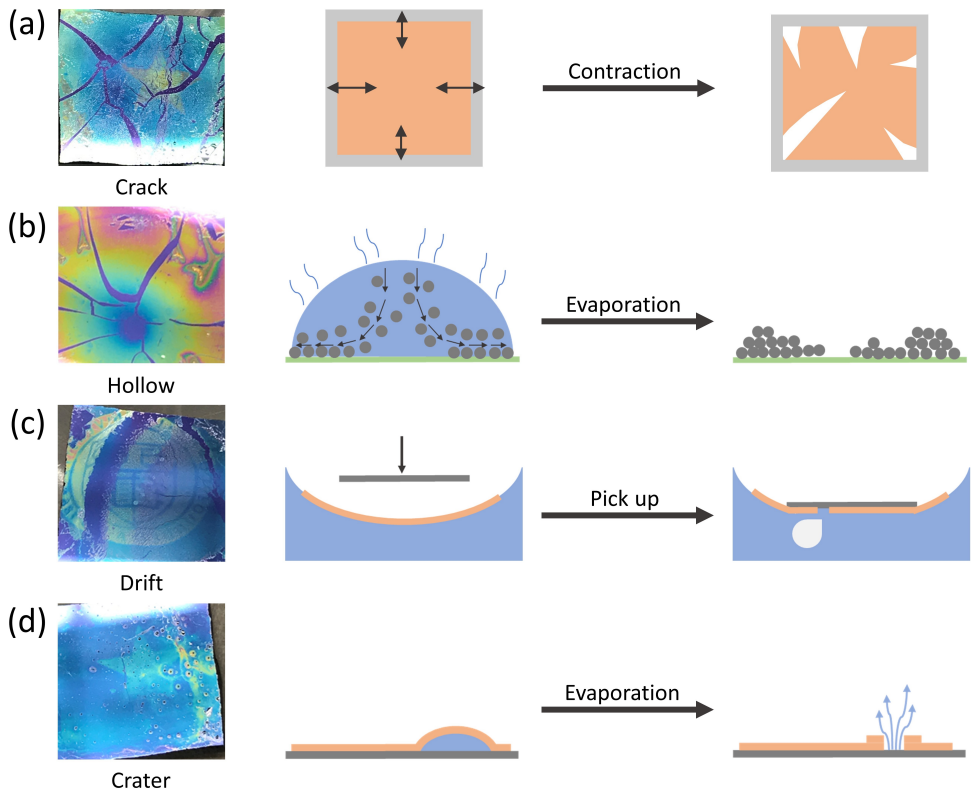

Figure 2.7: Formation mechanisms for different defects: a) cracking, b) hollowing, c) drifting, d) cratering.

the periphery of top phase is dry before it touches the wall. This will leave the top phase a free moving margin, so it is safe from tearing. The second type of defect, hollows, is because of the rapid evaporation of top phase solvent. The top phase is injected onto interface as droplets. At the beginning, the middle of the top phase will be thicker than periphery part, and then starts to relax until homogeneous thickness is achieved by spreading. At this stage, if the evaporation is too fast, there will be tangential flows of materials, which carry QD in the middle of droplets and deposit them onto the periphery regions. This effect results in a 'coffee ring' like structure (Figure 2.5b). To circumvent this effect, the Ill must be covered with a lid right after injection of top phase, to ensure that top phase fully spreads before it evaporates. The third defect is called drift. It was observed after picking

up an intact film from the fluid interface. Therefore, the cause is attributed to the air trapped betIen the substrate and the film. As the two parts contact with each other, trapped air can break the brittle film and escape, leaving a drifted pattern. To avoid this defect, the Teflon Ill should be large enough to ensure a flat fluid surface, so the contact betIen the substrate and the film is parallel and no air can be trapped. The fourth defect is called craters. It was observed after drying of an intact pattern successfully picked up from interface. EG droplets remaining on the wafer can penetrate through the film to touch the surface of wafer. When it evaporates, it will push the film on top of it aside, causing crater like defects. In order to avoid such defects, a methanol developing step is required after picking up film. The substrate is rinsed with methanol until all the EG is removed, and then put into a vacuum chamber to let the methanol fully evaporates.

With all these defects identified, the SOP is further improved with more details, including critical spreading and evaporation profile of ink, size of Teflon Ill, lid cover, developing steps, and functionalized substrates. These optimizations of SOP are critical in producing consistently homogeneous films, especially for further thickness related quantitative measurements.

Exposure Time

The quality of the patterns will increase at first, because of the oriented attachment reaction inside exposed area, and then decrease, due to diffusion of chemical trigger. A set of patterns Ire fabricated with different exposure time (Figure 2.6b), to find the optimal point where the pattern is formed, and thus reduce the printing time. Therefore, in an actual 3D printing scheme, each layer will be alloId to be exposed for this optimal time length. I found that, if exposure time is less than 6 min, the pattern can hardly be identified. At 6 min, the pattern can be seen, but not fully

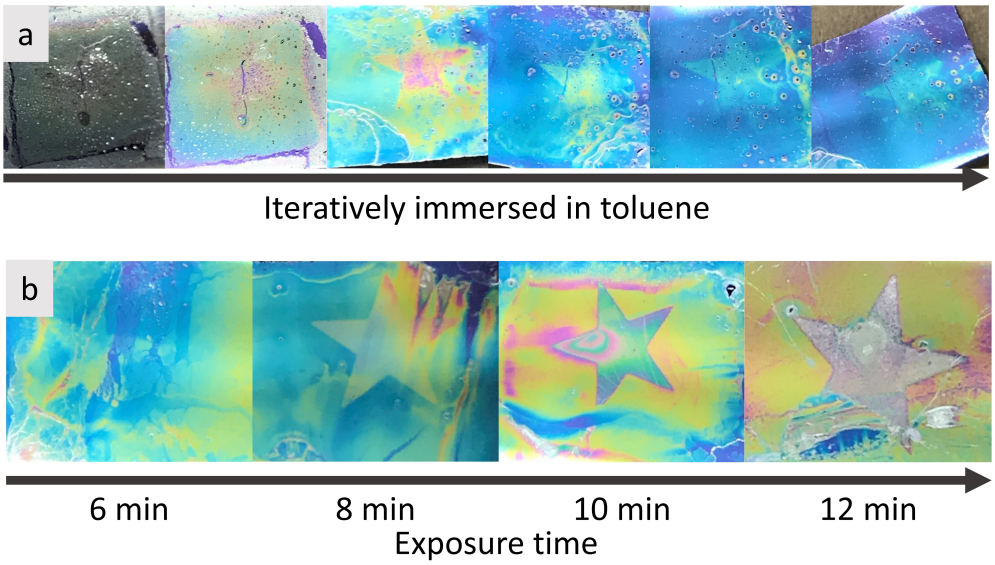

Figure 2.8: Effect on film quality with a) iterative immersion with sovlent and b) exposure time.

formed. After 8 min, the patterns have good qualities without blurring, which means the diffusion of ethylene diamine does not affect film resolution in minute time scale. Since then, 8 min was determined as the optimal light exposure time, and the following patterning are carried out based on this time.

2.4 Structure and Properties as a Function of Time

2.4.1 Ligand Shell Mechanistic

To get mechanistic understandings of how the proposed synergistic reaction is taking place, the processed films with different reaction time are probed with FTIR ex-situ. Each film was processed with the setup described above, and post-processsed with methanol only. As shown in 2.9, the peaks from 2800 to 3000 cm^{-1} are attributed to oleic acid hydrocarbon chains, and the peaks at 1550 cm^{-1}

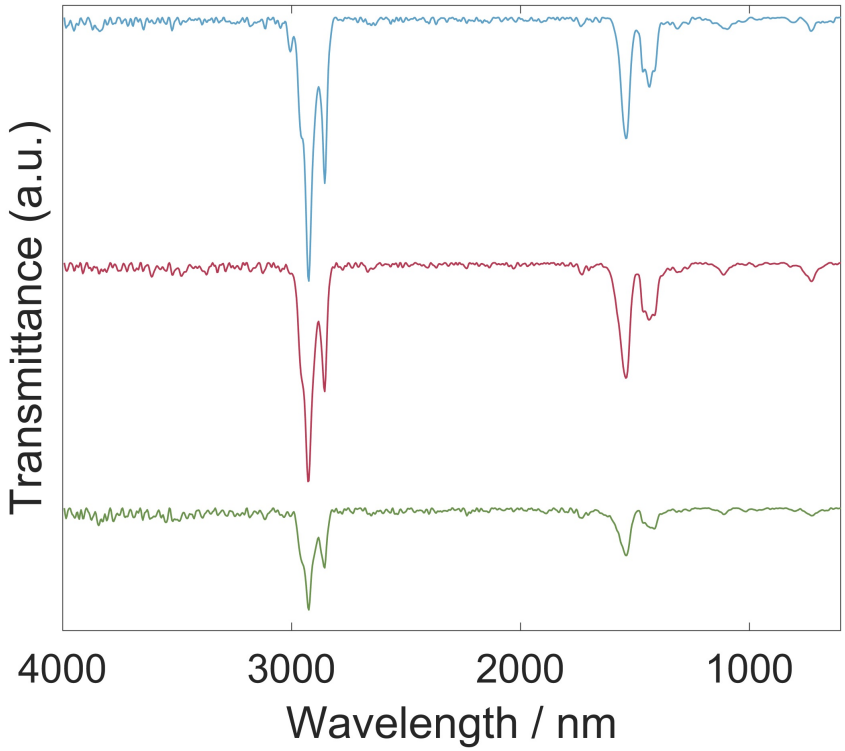

Figure 2.9: FTIR spectrum of films with different exposure time.

are considered from Cd carboxylate. Without any other peaks detected, it can be concluded that there is no ligand exchange during the process. The ligand coverage drops to 83.8% at 4 min and 37.8% at 8 min, by integrating the peak values. With the data discussed above, a mechanism which is limited by the release and transportation of EDA is proposed.

2.4.2 Optic Properties

Absorption

As patterning of CdSe QDs has been successfully demonstrated, whether the unique optic and electronic properties can be conserved still needs to be figured

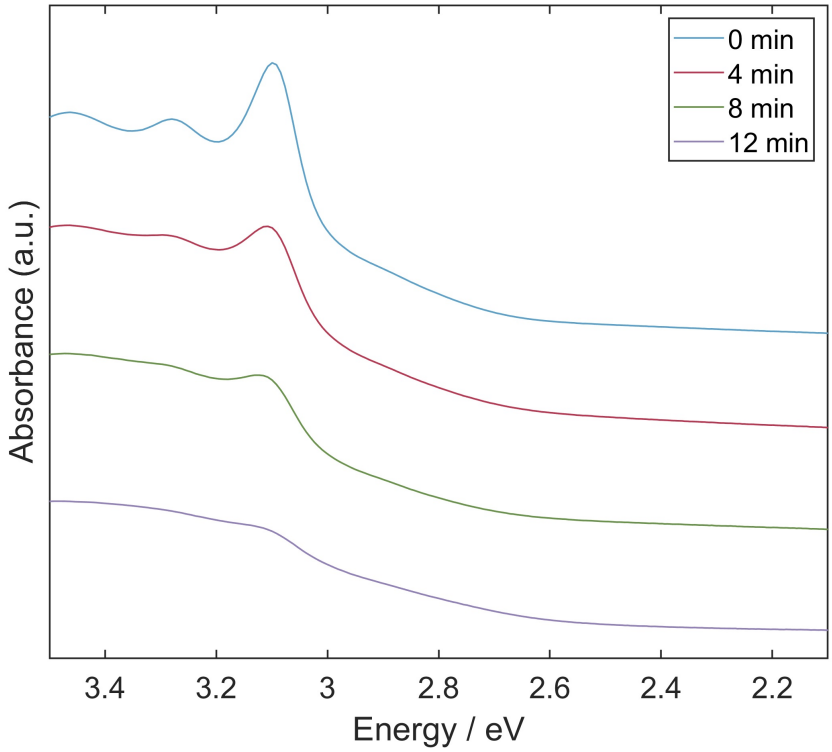

Figure 2.10: UV-Vis absorption spectrum of film with different exposure time.

out. Therefore, the UV-Vis spectrum of film with and without light exposure Ire studied (2.10). CdSe QD film, if drop coated on quartz slide, has a characteristic first absorption peak at 405 nm. This is identical with CdSe QD solution. This shows that QD optic function is conserved after solvent evaporation. The peak disappears after rinsing with hexane, which is a solvent of the oleate coated QDs. This is simply because CdSe QD can re-disperse back into hexane. The same behavior is observed when drop casting colloidal CdSe QD onto subphase I used for patterning, without light exposure. Same experiment was done by drop casting colloidal CdSe QD onto subphase, and exposing with UV light for 8 min. The characteristic peak of its absorption spectrum is conserved after hexane rinse. This indicates a solubility reduction caused by losing oleate surface ligand, but the core function is conserved.

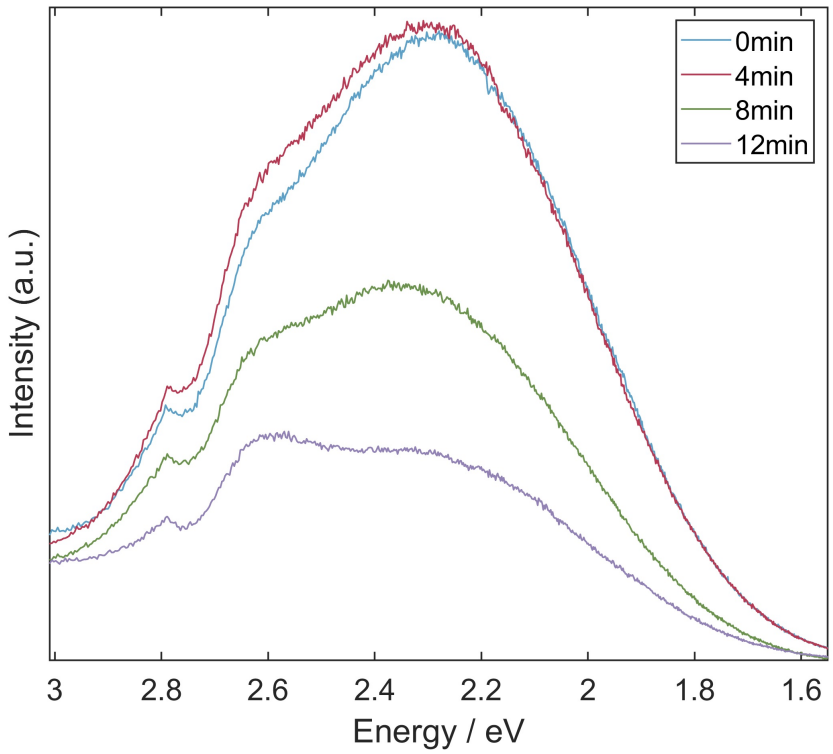

Figure 2.11: Photoluminescence spectrum of films with different exposure time.

Meanwhile, another interesting finding caught my attention. The pattern also shows both a substantial decrease in absorption peak height, and a peak width expansion. Considering the film thickness of this pattern is about 300 nm, it is very likely that the chemical trigger cannot react with the entire film due to diffusion limit. The QD layer will have a gradually decreased ligand coverage, as the distance to the interface is smaller. Therefore, QDs far from interface will still possess enough solubility to be re-dispersed back into hexane. Such behavior inspired me to seek for a kinetic model to quantitatively describe the transport-reaction mechanism. It gives information about resolution in x-y plane, and in z-axis (layer thickness).

Emission

With this transport-reaction scheme identified, thinner pattern was fabricated and characterized to magnify the impact of reactions closer to the interface. The photoluminescence curves of patterns after different exposure time Ire collected (Figure 2.9a), by illuminating samples with a 300 nm laser light source and scan emission across spectrum. The curves show three peaks roughly at wavelength 443 nm, 471 nm, and 539 nm (2.79, 2.63, 2.32 eV respectively). When splitting those peaks, each peak was assumed to be gaussian and a gaussian mixture fit Ire applied to the curve (2.11). The peaks at 443 nm (2.79 eV) are considered as band-edge emission. Its decrease over time can be explained by the degradation of semi-stable dots upon ligand stripping. It has been Ill demonstrated by other researchers that the peak at 539 nm is due to trap emission caused by selenide vacancies on CdSe QD surface. The ratio of band-edge / trap emission increases over exposure time. Since the dots I synthesized are Cd rich, which means there are intrinsic Se vacancies on the surfaces. An L-type ligand stripping triggered by photo-released ethylene diamine, which removes the oleic acid ligand together with the Cd binding site, will shift the QD surface from Cd rich to neutral, and thus suppressing the Se vacancy trap emission. The peak at 471 nm (2.63 eV), cannot be fully explained. There should be a third emission mechanism and trend of the ratio of this emission to trap emission can be discussed.

As a correlated optic behavior, the UV-Vis spectrum of patterns after different exposure time Ire also collected. The UV-Vis spectra show first absorption peak at 3.09 eV (401 nm), with negligible peak position shift but a significant peak broadening (Figure 1b). Considering the film is multilayered, the transformation from coated to bare QDs across the film cannot be homogeneous. In addition, I prepared a thicker film with the same setup and rinsed it with toluene after light

exposure. As suggested by the UV-Vis results, there are some unreacted dots that can be removed with toluene rinse, and for the rest part the quantum confinement is conserved. Therefore, three stages of the whole reaction scheme are proposed, including OA-coated dots, bare dots, and decomposed dots. Whether there is another stage betIen stage two and three where other organic molecules are attached to the QD surface needs to be ruled out.

2.5 Methods

Sacrificial Dot Synthesis. The sacrificial CdSe dots were prepared using the method described by Curtis et al. In a 50 mL round bottom flask connected to a Schlenk line, 1.28 g (10 $mmol$) of CdO and 10 mL (8.95 g) of oleic acid were added. The contents were heated to 50 $°C$ and mixed with a 2 cm stir bar at 1000 rpm. At 50 $°C$, the suspended mixture was placed under N_2 gas and the flask was heated to 140 $°C$. The CdO takes roughly 1-2 hours, at 140 $°C$, to react completely with the oleic acid and makes a translucent and viscous tan-orange solution. Once fully reacted, the solution is cooled to 90 $°C$. At 90 $°C$, the mixture is placed under vacuum to remove the water produced from the reaction. Note: This step is very sensitive to the vapor space and temperature. Below 90 $°C$, the mixture is too viscous for bubbles to break and above 100 $°C$, the vapor pressure is too high and the solution bumps. While under vacuum and bubbling is under control, the solution is heated to 120 $°C$. When bubbling subsides, the flask is cooled to 50 $°C$ and placed under N_2 gas.

In a 20 mL scintillation vial in a glove box, 1.00 g (12.5 $mmol$) of elemental selenium (powder) and 5.0 mL (4.15 g) of tri-n-octyl phosphine are added. The contents are mixed with a 1 cm stir bar at 1000 rpm. Caution: Heating the mixture

may prevent complete dissolution of the selenium, as selenium is known to form insoluble polymorphs. Once fully dissolved, the vial can be brought out of the glove box.

While the CdOl solution is at 50 $°C$, 2.0 mL of the 2.5 M TOPSe solution is injected into the 10 mL of 1.0 M CdOl solution. The solution is mixed for 5 min to ensure a homogenous concentration. The solution is then heated to 80 $°C$ over a 20 min period. Once the temperature reaches 80 $°C$, the mixture reacts for 120 min. After which, the reaction is quenched with 10 mL of ethyl acetate, which produces a white fibrous precipitate. Cleaning of the sample is done through centrifugation with hexane (or toluene) as the solvent and ethyl acetate (or ethanol) as the counter solvent.

PbS Synthesis. The PbS quantum dots were prepared following a modification of the Hines method. 0.45 g lead oxide, 10 g oleic acid, and 10 g 1-octadecene were mixed in a 100 mL round bottom flask and heated to 110 $°C$ for 20 min under vaccum to obtain a clear solution. The temperature was adjusted to the desired injection temperature (95-185 $°C$) followed by a fast injection of 210 μL of $(TMS)_2S$ diluted in 5 mL of ODE. Immediately before injection, the heating mantle was removed and the solution cooled naturally after the injection. When the reaction solution reached 30 $°C$, 30 $\mu L$of raw solution was removed and dissolved in 2.5 mL of TCE for adsorption measurements. Before device fabrication, the PbS QDs were purified twice using hexane and ethanol and redispersed in octane at a concentration of 40 mg/mL.

Semiconductor Matrix of Sacrificial CdSe Dots. 60 mg PGEDA and 140 mg ascorbic acid, and 10 mL ethylene glycol were mixed in a 20 mL vial and sonicated for 2 hours to obtain a clear solution. 750 μL of as-prepared solution was added into a $1.5 \times 1.5 \times 1.5$ cm^3 teflon trough to form a subphase with an

upward curvature. Then 18 μL of 4 mg/mL CdSe dot colloidal solution in hexane were dropped onto the fluid interface and the trough was immediately covered with a glass slide. After a complete evaporation of top phase solvent and formation of a shinny layer of CdSe dot, the glass slide was removed and a light source of wavelength 385 nm was imposed onto the interface for 0-12 minutes.

To further tune the thickness of CdSe film, the concentration of top phase can be tuned. However, with increasing concentration of the colloid, the increasing viscosity should also be taken into account with regard to spreading issue.

Sample Transfer. Samples were first prepared at fluid interface with the method described above. Then samples were transferred onto a desired substrate for further measurements or characterizations. Desired substrates include: 1×1 cm^2 slice of quartz slide for UV-Vis / Photoluminescence measurements, 1×1 cm^2 slice of undoped silicon wafer for FTIR / Profilometer / SEM measurements. Samples were subsequently washed with methanol to remove remaining subphase solution on the substrate and placed in an vacuum chamber for 1 hour to remove any remaining solvent before any other characterization.

CHAPTER 3

METAL-ORGANIC POLYMER TO SEPARATION DEVICE

Abstract. Coordinate polymers are promising candidates for size-selective separation applications, because of the micropores precisely defined by coordination chemistry. Here, I present a facile fabrication technique of hierarchical porous structures with metal-organic polymers. Acrylated zirconium oxide clusters are formulated as ink for 3D printing of programmable superstructures. Further studies about the pore size distributions reveal that the superstructure possess pores with size spanning from sub-nanometer to a few micrometers. I show that the pore size distribution can be modified by different mechanisms from synthesis to assembly and a process-structure-performance relation was established to guide the design of devices. Then a separation column was prepared by this materials for a liquid phase separation of drugs and carcinogenic impurities. A hierarchical porous structure greatly facilitate the separation process with the micropores removes impurities by trapping and mesopores allows efficient diffusion of mass into the porous media. Finally, a successful purification of drugs was conducted.

3.1 Introduction

Hierarchical structures are ubiquitous in the nature. For example, trees possess hierarchical water flow systems, where the main channel in the trunk carries large amount of water from ground to crown, the branched channels spread the flow to leaves and the terminal microchannels delivers water to specific cells. During the water delivery inside plants, structures at different level of hierarchy function differently, from pressure driven flow to concentration driven osmosis.

Microporous materials possess important potential technological implications spanning storage, separation and catalysis.[53] However, the absence of monolithic forms significantly limits their mass transportation and thus practical applications.[34, 24] In general, separations using microporous materials are carried out using powdered materials in a low-throughput manner, leading either to a throughput-selectivity trade-off or high back pressures.[47] Notably, high throughput and selectivity can be achieved simultaneously in natural systems by hierarchical design.[44] For example, intestines utilize macroporous channels to enable transport of nutrients and nanopores to enable adsorption of these nutrients. Nonetheless, our ability to fabricate microporous materials into structures analogous to natural hierarchically design is still in its infancy.

Concurrent advances in the nanostructured building blocks[26] and optical patterning[13] have opened opportunities to program materials over multiple length scales. Assembly of colloidal nanoparticles is an attractive strategy to produce hierarchical structures.[42, 39, 41] Studies using molecular ligand-ligand interactions, such as organic ligands or DNA, to directionally bind and orientate nanobuilding blocks have generated nanoscale features including mesopores and macropores.[21, 22, 38] On the other hand, advances in photoresponsive ligand chemistries have created new prospects to spatially pattern assemblies by light.

Recent works have demonstrated the fabrication of hierarchical nanoporous materials by combining nanoparticles' assemblies with light-initiated 3D printing.[28, 49] However, this strategy has so far been rarely used for the formation of microporous materials, as the formation of sub-nm features from nanoparticle assemblies has not been realized.

In this chapter, I will discuss the findings to accomplish hierarachical control over microscopic porosity, mesoscale assembly, and macroscopic superstructures, which leads to new materials exhibiting efficient mass transport and selective adsorption of NDMA. The directional connection of colloidal building blocks at the molecular level to generate micropores are observed. The formation of sub-nm pores is validated by demonstating the removal of NDMA from the drug Irbesartan. This promising technique enables control of pore size on the ångström level for size-exclusive separations as an alternative to the recent focus on tuning chemical functionalities to separate species by polarity.

3.2 Photoresponsive Ligand on Inorganic Core (PLIC)

Additiva manufacturing, also known as 3D printing, has emerged as an effective bottom-up approach to enable the design of complicated macroscopic geometries. Digital light processing (DLP) 3D printing has been of interest for the rapid print speed, high resolution and low cost. It utilizes photoresin as the basic building blocks. However, most photoresins are organic compounds based on hydrocarbon backbones with functional side groups. The structures obtained with these photoresins often lack precise microscopic order and functionalities. Therefore, for real applications in catalysis, optics and electronics, composites of these materials and other functional parts are needed. Coating the surface of an inorganic core with

photoresponsive ligands opens a broad opportunity to directly fabricate functional assemblies. With photoresponsive ligand on inorganic core (PLIC) as the ink for DLP 3D printing, the structure formed can be spatially programmed *in-situ* to create inorganic/organic hybrid materials with the intrinsic functionalities designed by the synthesis of PLIC ink.

Zirconium oxide clusters $Zr_6O_4(OH)_4(MAA)_{12}$ (Zr-MAA) are functionalized with methyl methacrylate as a colloidal building block to fabricate hierarchical porous materials. Before fabrication, the clusters are dissolved in toluene together with photoinitiator (diphenyl(2,4,6-trimethylbenzoyl) phosphine oxide) as a photoresponsive ink. Exposing this formulation to UV light triggers polymerization of the methacrylate groups and forms robust connections between constituent building blocks. When combined with (digital) light patterning and additive manufacturing strategies, this approach can form arbitrary shapes by moldings or patterned UV light sources. In an important distinction from prior work regarding coordination polymers, building blocks are based on monodentate ligands ending with photoresponsive groups (C=C) instead of active chelating groups. Photoinitiating the reaction leads to formation of micropores, mesopores and macroscopic structures in a single step. Therefore, the colloidal Zr-MAA nanoclusters are stable and processable in solvents before any pores have formed. The materials fabricated using our approach share some similarities with porous coordination polymers (PCP).[18] For PCP, micropores are formed first via the connection of multidentate organic linkers with inorganic cores, which then react further to form larger structures. However, the inherent fragility limits the synthesized micropores to powdered form, leading to notoriously challenging processing.

3.3 Hierarchical Porous Structure

Similarly, inspired by the nature, hierarchical structures are employed in preparation of functional materials, such that different functions can be incorporated into one device to tackle complex tasks.[16] Hierarchical porous structure of MOF can be created utilizing the thermal instability of linkers.[54] By doping thermally unstable linkers into the MOF crystal, a thermolysis step after crystal growth removes the unstable linkers and the local structure will collapse into mesopores.[17] These mesopores can facilitate the mass transport in the porous media and improve the efficiency of transport related applications, such as capture and catalysis. Instead of linker labilization, pores with different size can also be fabricated by crystallization of MOF on a porous template. This structure has been used for enzyme immobilization that larger pores encapsulate enzymes and smaller pores control the mass feed to react with enzymes.[29] The hierarchy in porous media is intriguing, promising and challenging, since it grants the structure with multiple functions and tunable properties at different length scale. The mechanistic understandings of each hierarchy level are important for structural design and device fabrication. In this work, the formation mechanisms of different pores are discussed. The micropores are related with coordination geometry of inorganic clusters and organic linkers, and can be tuned by molecular design. The mesopores are formed by stacking of fractal clusters and gelation, and the pore size distribution can be controlled by reaction kinetics. The macropores are designed with respect to applications and realized by a digital light processing (DLP) machine.

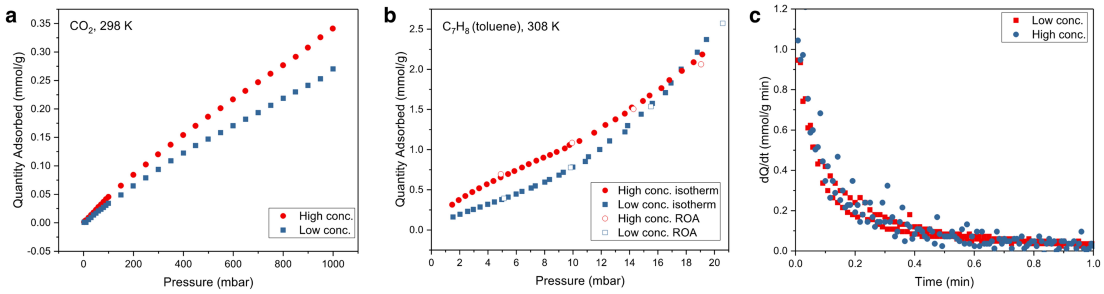

Figure 3.1: a) CO_2 sorption isotherms at 298K, b) toluene sorption isotherms at 298K, c) rates of toluene adsorption on superstructures with different pore size distributions.

3.3.1 Micropores for Angstrom-precise Separation

When acrylated Zr clusters are connected through radical C-C coupling of methacrylate ligands, the size of micropore window formed are precisely controlled by the coordination symmetry of Zr oxide clusters and the size of methacrylate dimers which links two clusters. To validate the permanent porosity, we probed the adsorption of different gases. Carbon dioxide (2-3 Å) uptake was measured (3.1 a). The result confirms that the sample made from a high concentration of Zr-MAA can uptake more CO_2 because of more micropores. However, both of the samples possess relatively low CO_2 capacity (¡ 0.4 mmol/g) due to the absence of strong CO_2 binding sites. Complementary gas uptake experiments with toluene (5-6 Å) conducted reveal a gas uptake (3 mmol) that is seven times higher compared to CO_2. Since there is no adsorption sites that selectively interact with toluene, it is likely that the stronger interactions between toluene and the pore walls than CO_2 comes from steric effect, which means larger toluene can be trapped more strongly within the 6 Å micropores (3.1 b). The validation of trapping behavior of micropores towards smaller molecules form the fundation of size-selective separation. Importantly, the observed micropores unveil an unreported chemistry to utilize acrylate monomer ligands to oriented attach inorganic nanoparticles, which

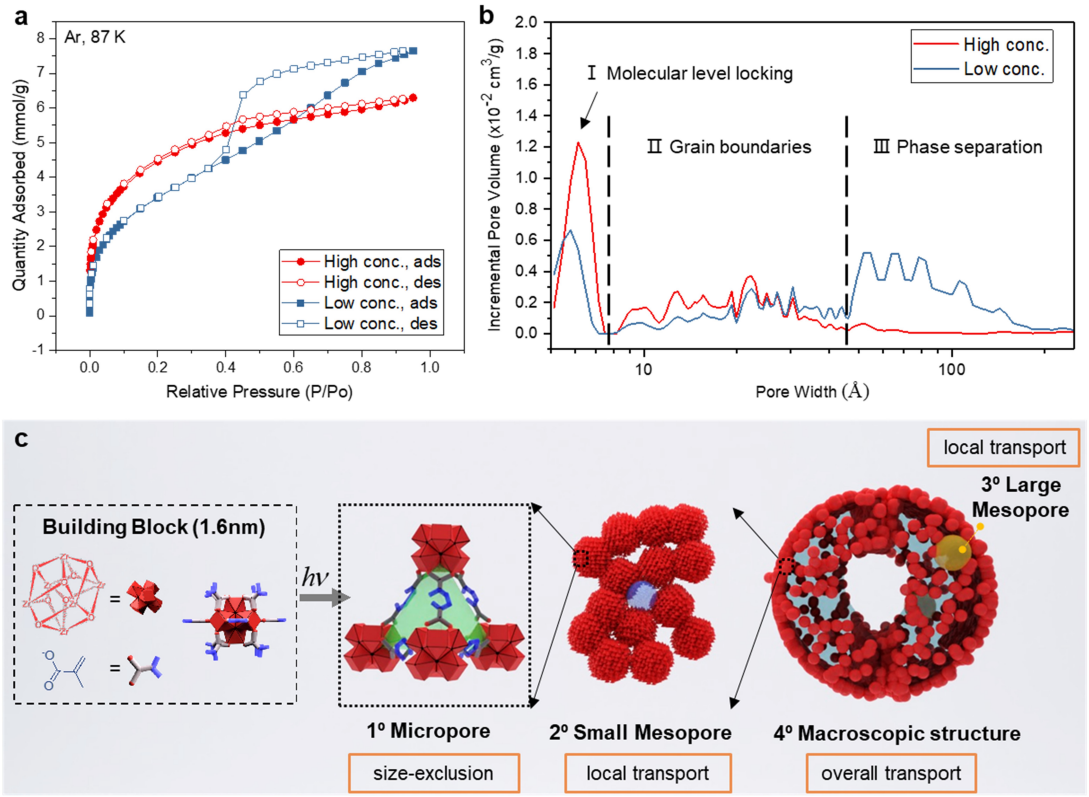

Figure 3.2: Gas adsorption measurments and multi-scale pore size analysis. a) Argon sorption isotherms with samples prepared in high and low concentration of building units, b) Pore size distributions, c) Proposed hierarchy of multi-scale porosities.

is different from bulky photopolymerization. The 6 Å pores can be referred to as tetrahedral cages similar to the tetrahedral cages of UiO-66;[27, 5] however, we cannot rule out the formation of octahedra at this time. We infer that the kinetics to form tetrahedral cages are faster than forming octahedral cages, so the building units incline to stack into tetrahedra.

3.3.2 Mesopores for Transport

The pore size distribution was analyzed by Ar gas adsorption (3.2). The step-like desorption behavior of the isotherm in 3.2a is indicative of mesopores within the

material. When dense liquid phase in mesopores are evaporating, the capillary force slows the evaporation rate and cause hysteresis. 3.2b shows the hierarchy of pore sizes spanning from Å sized micropores (region I), several nm (region II) to tens of nm (region III) sized mesopores. The first distribution is in the micropore regime (6 Å), as described above, arises due to the connection of building blocks similar to the structure of UiO-66.[19]

The second pore-size distribution is around 2-3 nm. We attribute these pores to the space between superclusters of linked tetrahedra; the superclusters visibile in scanning electron microscopy images are around tens of nanometers in diameter (3.3). The distribution of sub-nm pores (within the tetrahedron) and nm pores (between the superclusters) hence reflects the nucleation and growth conditions. The growth of Zr-MAA nanoclusters into a single, large crystal is difficult because of the relatively fast kinetics and irreversibility. The third pore-size distribution is in the range of ten nanometers, which we attribute to phase separation behavior during material processing. Large mesopores like the ones formed here have been previously observed using the same $[Zr_6O_4(OH)_4]^{12+}$ cluster under hydrothermal conditions.[9]

The relationship between the broad spectrum of pore sizes is schematically summarized in 3.2c. The pore-size distribution can be adjusted by changing the building block concentration. I hypothesize that this processing-structure relationship derives from the underlying nucleation and growth dynamics of the tetrahedra and superclusters. A high concentation of building blocks leads to enhanced nucleation of superclusters whereas low concentration of Zr-MAA leads to less nucleation and more growth to form larger superclusters and hence a more dominant contribution of nm pores in the final material. The ability to control hierarchical porosity can greatly mitigate mass transfer limitations, increasing the likelihood of small

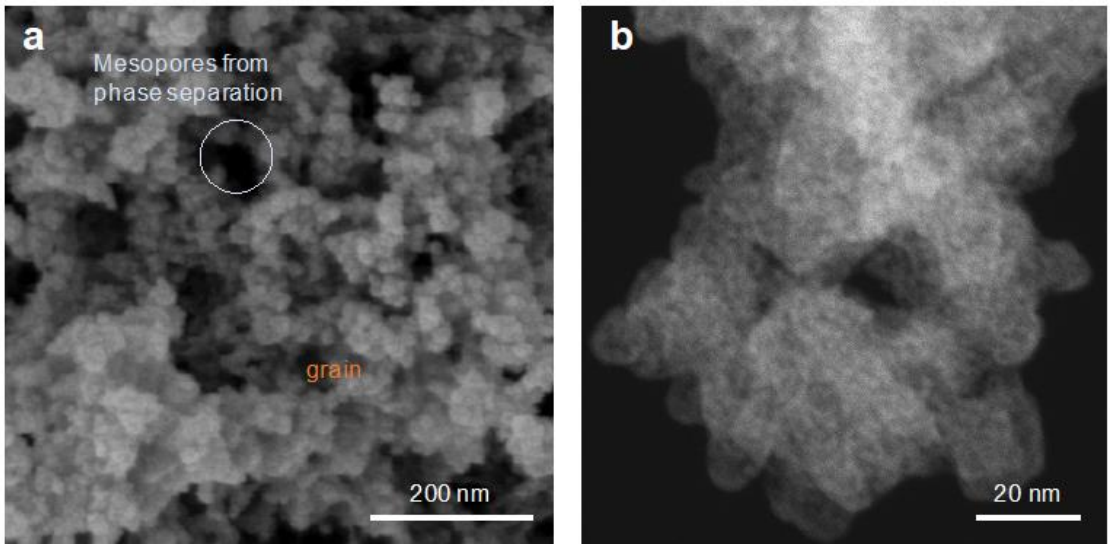

Figure 3.3: a) SEM image showing grains and tertiary mesopores made from phase separation. b) TEM image showing grains in detail and spacing between them.

molecule adsorption in the micropores.

3.3.3 Macropores for Throughput Channel

In a mesoporous media, the mass transport are dominated by diffusion due to capillary force and narrow branched channels. The mass flow will be greatly accelerated with effective convection in the system. Natural strucutres like leaves utilize a wide main channel to deliver mass to subordinate parts with fast convection flow, and then the mass diffuses in to react. Similar structured separation columns can be fabricated with DLP 3D printing. Instead of slow diffusion through all column, a millimeter sized channel in the middle of column accelerates the flow rate by over 100-fold. With such advances in fabrication, the applications of PLIC material in liquid phase separation are tested.

3.4 Size-selective Liquid Phase Separation

The ability to design and implement hierarchically porous materials presents compelling prospects to address challenging purifications. Combining intrinsic micropores for host-guest interactions with interconnected meso/macropores for enhanced mass transport can uniquely open up angstrom-precise size-selective separations. One specific and urgent separation challenge that could benefit from this approach is the removal of carcinogenic contaminants from generic pharmaceuticals. NDMA, a member of the N-Nitrosamine family and a potent carcinogen, has been discovered in multiple generic drugs including angiotensin II receptor blockers (e.g. irbesartan, valsartan), ranitidine, and potentially metformin.

Conventional approaches fall short of addressing the challenge of removing NDMA from pharmaceuticals. NDMA is resistant to air stripping due to its high solubility and polarity. In addition, commonly used strategies of separation based on ion strength or hydrophobic interaction are both ineffective, because nitrosamines are neutral at pH ranging from 4 to 10 and have weakly hydrophobic interactions with sorbents. Last, current size-exclusion separations are primarily limited to larger molecular weight species (¿10 kDa) and do not provide enough resolution to remove NDMA from other small molecules. Therefore, new strategies are needed for the selective removal of NDMA from contaminated pharmaceuticals.

3.4.1 Separation Column for Relieved Backpressure

Having established the relationship between processing conditions and pore size distribution, I set out to test the performance in chemical separation applications. The fabrication of these meso-scale porous materials can be combined with light

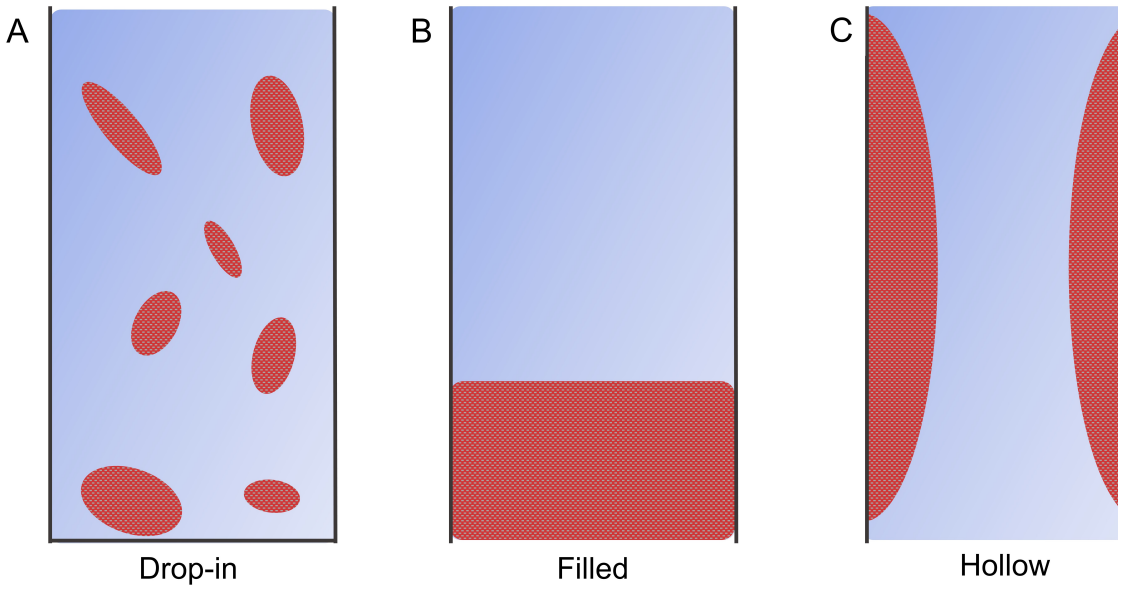

Figure 3.4: Separation column design: a) drop in, b) fully pacled, c) hollow.

processing approaches to create stuctures in which flow channels can be defined from the μm to cm scale. I started by dropping pieces of printed porous materials into a mixture solution of drug and NDMA (3.4a). After stirring, the loose pieces were removed by centrifuging and the supernatant was monitored with UV-Vis absorption. However, the unreacted monomers will introduce additional impurities into the system, with an absorption peak around 230 nm, confirmed by absorption spectrum of ethanol that flows through the material (3.5b). Therefore, unreacted PLIC clusters remaining in the printed structure need to be removed before separation can be conducted. Then, I printed a micro/mesoporous monolith fully in a syringe similar to a solid phase extraction setup (3.4b). Separation experiments to remove NDMA showed a reduction in the carcinogen level from 5% in the inlet feed to 0% in the outlet (3.5 and 3.5), which validates the use of superstructures for angstrom-precise size separation. However, even given the exceptional hierarchy of large and small mesopores to help transportation, the flow rate through monolithic structures is still limited to around 1-2 ml/hour due to high back pressures, which

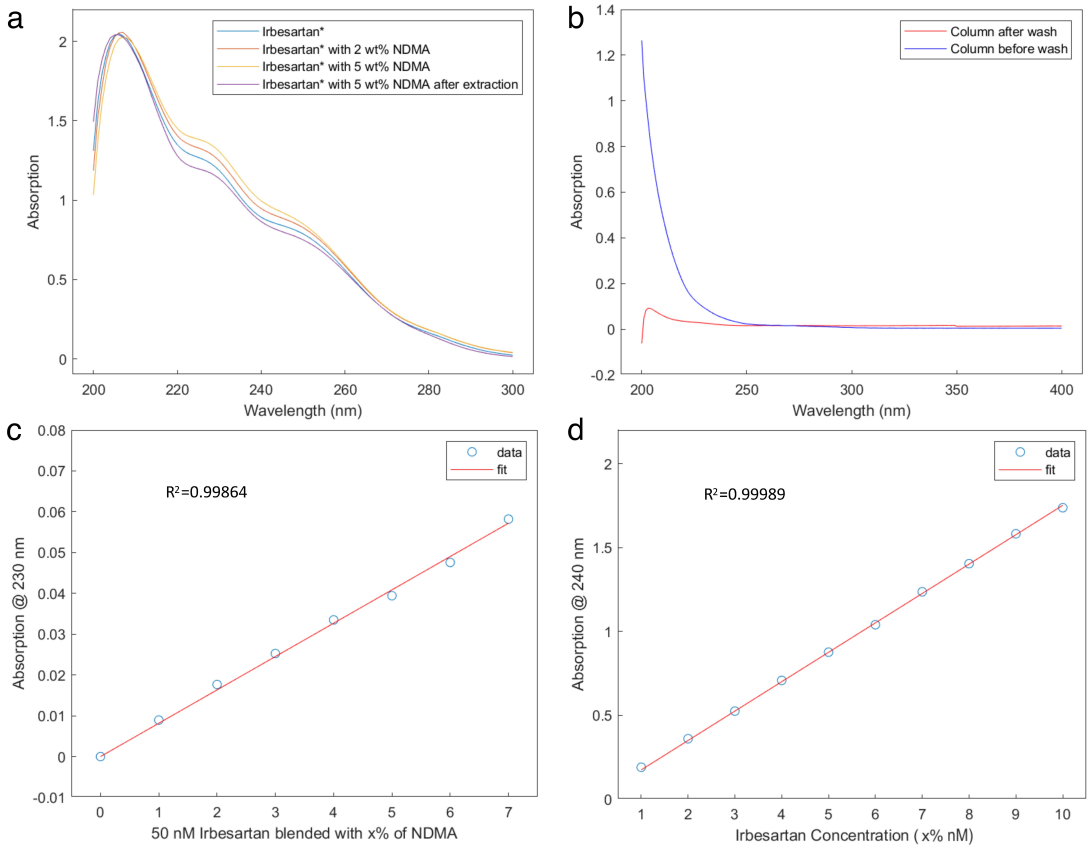

Figure 3.5: Uv-vis data of a) different concentrations of NDMA before and after separation, b) devices before and after wash, c) and d) shows the linear consistency of Irbesartan and NDMA's concentration.

is the critical bottleneck for almost all separation technologies.

The freedom to fabricate complex shapes using proposed processing method is leveraged to explore different macroscopic structures to resolve the backpressure challenge. Inspired by hierarchical design present in nature, we adopted a structure similar to that of an intestine. This more efficient design increases the flow rate from ml/hours to ml/minutes. A hollow tube superstructure (akin to a hollow fiber membrane commonly used in separation processes, 3.4c) was fabricated with the macroscopic channel for transportation, and the wall was used liked villi to absorb impurities (3.7a). 3.7b concludes the improvement in throughput by hierarchical design compared with the common fully-packed design. The removal efficiency of

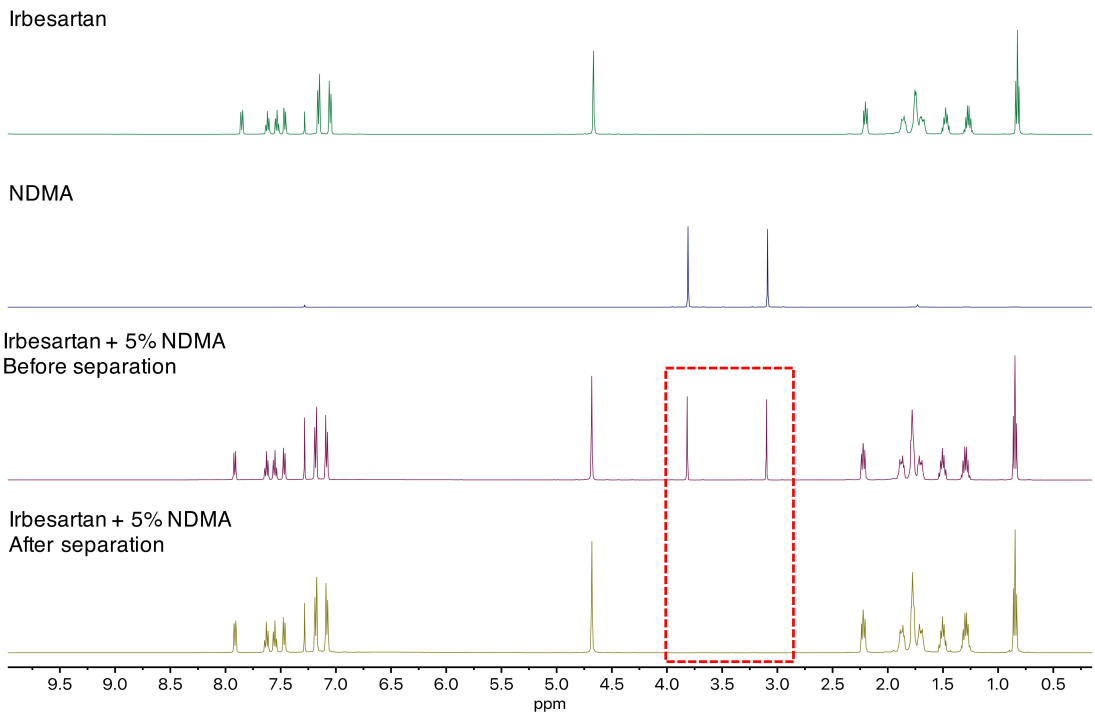

Figure 3.6: NMR of Irbesartan and NDMA before and after separation (full pack column).

hierarchically designed superstructures prepared with different concentrations of Zr-MAA were studied in 3.7c. Higher concentrations of Zr-MAA precursor shows better removal efficiency. The result is consistent to the gas phase studies supporting that more micropores help the separation performance. The optimized superstructure shows 93% NDMA removal efficiency after 9 cycles, bringing the concentration down from an initial 50 ppm to less than 4 ppm, at a flow rate of 2 ml/min, which is tens of times faster than the fully-packed design.

The removal efficiency with different initial NDMA concentrations (3.7d) and a simplified analytical model to explain boundary layer phenomenon. The results highlight the importance and potential to achieve contradicting throughput and performance at the same time by rationally designing in macroscpoic scale. To date, relatively few studies to date have taken macroscopic design into considera-

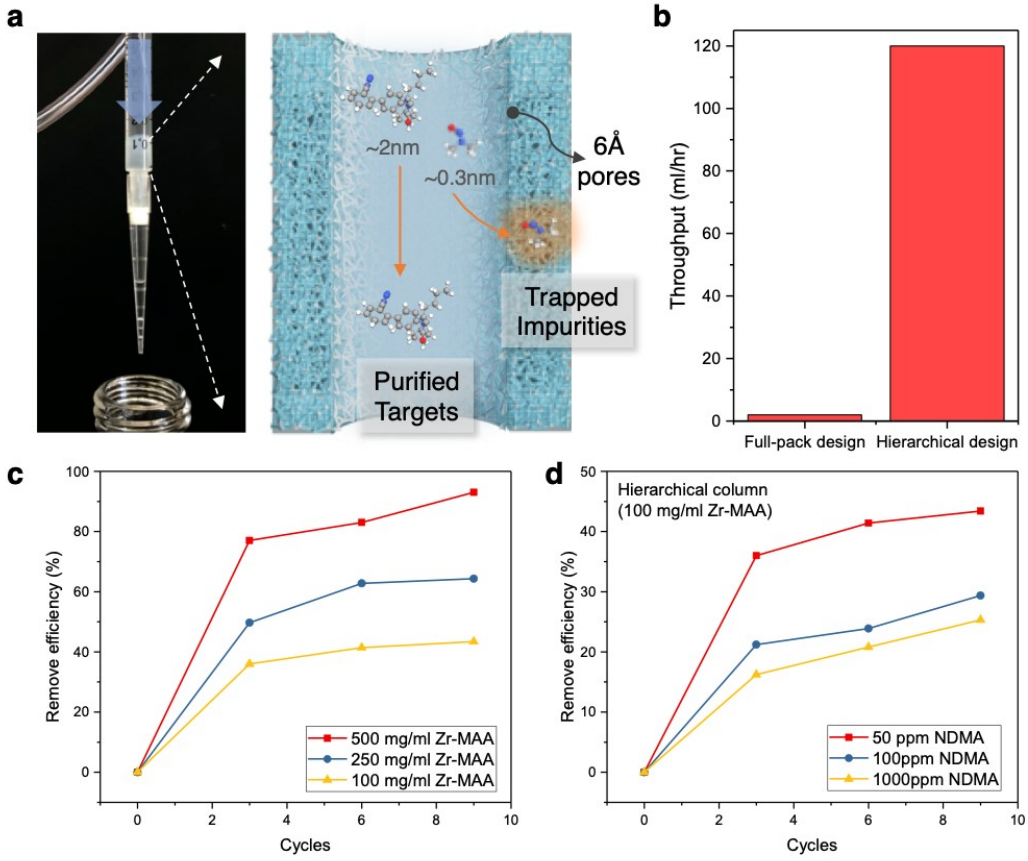

Figure 3.7: Ångström precise separations with hierarchical design: a) device setups for the carcinogen removal in recent recalled drugs: syringe filled with superstructures, b) Throughput comparison of hierarchical design and full pack design columns. Removal efficiency of c) columns prepared with different concentration of Zr-MAA and d) different initial concentration of NDMA contaminates.

tion because of the insufficient processing approaches available.

Separation Efficiency

I tested the yield and performance in the separation of the NDMA from a recalled batch of pharmaceuticals as shown in 3.8. On average, the recalled drugs surpass the FDA approved intake amount by more than ten times the limit. Thus, we did experiments with a mixture containing the Irbesartan drug and 10 ppm NDMA.

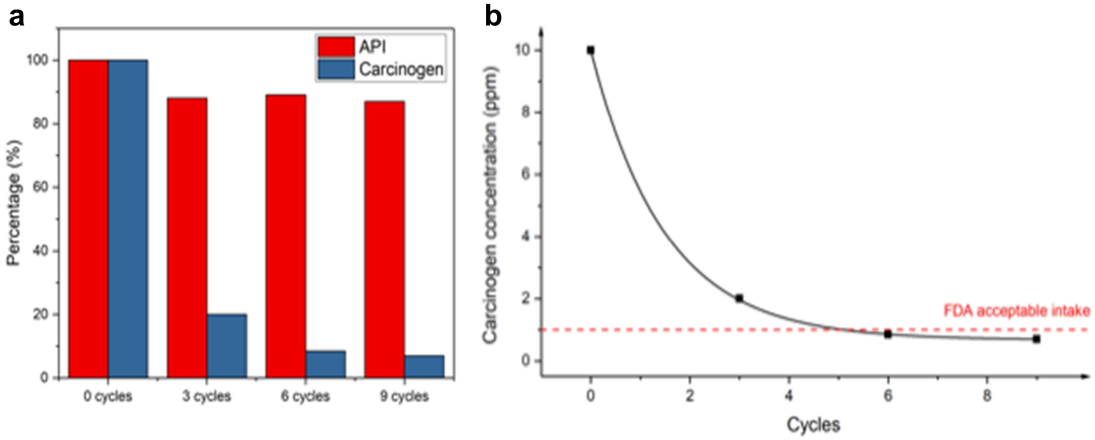

Figure 3.8: Contaminant removal efficiency: a) Yield of drug API and carcinogen impurity, b) The carcinogen concentration after a given number of separation cycles.

For each cycle, the mixture was flowed through the same separation column at a flow rate of 1 ml/min, when the mixture interact with the column walls to trap NDMA. The contaminates drop below FDA's average requirement, 1 ppm, after 6 to 9 cycles of separation shown in 3.8b. More importantly, the result was achieved selectively with only a 10% loss in the drug yield, as shown in 3.8a.

Our hierarchical device demonstrates an unique opportunity of "structured" microporous materials to become an energy-efficient, cost-effective and high-selective alternative for molecular separation processes. With the distinguishing features of solution processability in room temperature and selected low-cost precursors, the device can be fabricated on-demand within 5 minutes and tens of dollars. In addition to its simplicity, the device is readily adaptable for potential use in various pharmaceutical scenarios, such as an additional/combined processing step of chromatography or tangential flow filtration.

3.5 Methods

Building block synthesis. Zr-MAA was synthesized by the modified method previously reported.[46] Briefly, 1 ml of Zr isopropoxide was mixed with 1 ml of methacrylic acid in a flask. The flask was left opened for solvent evaporation to 1/2 of the initial volume, and the product was washed with 1-propanol. The final product was dried under vacuum.

Fabrication of superstructures. Ink was formulated by mixing dried Zr-MAA nanoparticles from the previous step with photoinitiator and solvent. For example, 100 mg of synthesized Zr-MAA, 1 mg of photoinitiator, diphenyl(2,4,6-trimethylbenzoyl) phosphine oxide, were added into 1 ml of toluene. Inks were purged with nitrogen flow for 2 minutes before usage. Samples for gas sorption measurements were prepared by a digital light processing projector operating with 385 nm wavelength light and intensities of about 10 mW/cm^2. Free-standing monoliths formed as a single layer by projecting the light pattern for 2 minutes directly on top of the Si wafer. Inks with 500 mg/ml and 100 mg/ml of Zr-MAA were labelled as high and low concentration.

General characterization methods. Powder X-ray diffraction characterization was carried out on Bruker-AXS D8 Discover Diffractometer using Cu Kα radiation at $\lambda = 1.54$Å by depositing powder onto glass substrate. The FTIR was conducted on Bruker Hyperion FT-IR Spectrometer & Microscope. A background scan was collected before each measurement (64 scans), sample scan was an average of 64 scans, and resolution was set 4 with a data spacing of 0.482 cm^{-1}. The concentration of NDMA carcinogen was measured by Shimadzu 2030 Gas Chromatography (GC) following the FDA's method. Generally, samples were held at 50 °C for 2 min, ramped from 40 °C to 100 °C at 5 °C/min, ramped from 100 °C to 220°C at 20 °C/min, ramped from 220 °C to 250 °C at 30 °C/min, and then held at 250 °C

for 2 min. ^{1}H NMR spectra were recorded on a Bruker AV500 spectrometer with 16 scans and 45 deg excitation pulse. NMR data was analyzed by MestReNova.

Gas sorption. Samples for gas sorption were washed and exchanged with methanol for 24 hours. Then samples were dried with supercritical carbon dioxide dryer (Leica CPD300 critical point dryer). Gas adsorption measurements were carried out using a Micromeritics 3-flex gas sorption analyzer and high purity Ar or CO_2 (99.999% pure).

Liquid phase separation. Ink with different concentrations of Zr-MAA was loaded into a cylindrical plastic tube, and then exposed with UV light (385 nm, 10 mW/cm^2) for 5 min. For hierarchical design devices, the ink was injected into a cylindrical plastic tube (radius 5 mm) with a needle (radius 1.5 mm) inserted in the middle. Then the tube was exposed with UV light. Once the superstructure formed, the needle was removed and the device was connected to a syringe pump. To clean the superstructure, ethanol was continuously flowing through and the UV-Vis spectrum of the outlet flow was monitored. After the adsorption peak of unreacted clusters and toluene reduced to zero, a mixture of API and NDMA was flowed through the superstructure iteratively and sampled. For example, a 5 ml ethanol solution of API (2 mg/ml) and NDMA (0.01 mg/ml) was flowed iteratively through the as-prepared column at a flowrate of 2 ml/min. After the outflow is collected, it was injected back into the column for another cycle. Every cycle, 100 μL was taken from the collected outflow for quantitative GC tests.

CHAPTER 4

CONCLUSION & OUTLOOK

Abstract. In this chapter, main conclusions of the works introduced by previous chapters will be drawn. In addition, new directions in the future will be proposed. These future works include projects that can be initiated within a few months, promising research topics in this field that may emerge within a few years, as well as future predictions about how this field will be over time length of decades.

4.1 Summary

In this section,the main conclusions I have demonstrated in the previous chapters will be summarized.

Quantum Dots as Building Blocks

In this work, I employed protected-EDA and CdSe quantum dots (QDs) to create a temporal and spatial EDA concentration profile via QD-catalyzed dissociation of protective groups and subsequent release of EDA. With the aid of this concentration profile, CdSe was successfully patterned with a two-phase setup. Then the reaction kinetics was investigated with FTIR spectrum and a kinetic model. It turns out that the surface oleate ligands are kept being removed , resulting in an organic-free CdSe film. By probing the optical absorption and emission properties, I found the CdSe QDs decompose to bulk material during the process. Finally, I demonstrate that when mix two type of dots with different stability, the more unstable can decompose and fill in the gap of the other one and create a interconnected hetero superstructure.

Inorganic Cores as Building Blocks

Hierarachical control over microscopic porosity, mesoscale assembly, and macroscopic superstructures are demonstrated, leading to new materials exhibiting efficient mass transport and size-selective adsorption of small molecule contaminants. Beyond the specific model system of NDMA removal in a hollow-fiber flow geometry, I envision that the concurrent advances in materials synthesis and photoprocessing enable a diverse range of hierarchical porous structures in which mass

transport and adsorption can be independently optimized. The emerging opportunities to assemble nanobuilding blocks to control spacing and architectures from ångström to centimeter scales by design allows for theorists and experimentalists to design and test novel porous materials. Hierarchically porous materials shown here solve recent challenges in attaining high purity and high flow rate at the same time. Given the broad library of inorganic cores, we foresee that this approach will inspire a number of novel device architectures. Our results and the hierarchical strategy proposed herein pave the way for pratical usages of structured microporous materials in emerging separation applications.

4.2 Perspectives

In this section, the significance and impact of this work to the field will be discussed.

Additive Manufacturing

In chapter 2 the ability to spatially deposit semiconductor materials at a fluid interface is demonstrated. Intuitively, stack of multiple layers on a build stage can extend this process into 3D. From the perspective of processing feasibility, there are several challenges to be tackled. Firstly, since each layer is fabricated on a fluid interface and controlled to be as thin as a few nanometers, it is challenging to transfer the layers without causing any defects, such as cracks, wrinkles, mismatches, etc. Standard work flow has to be established to guarantee a reproducible stacking of each layer. Steps may include transferring from fluid interface to substrate, cleaning of reactant residuals and annealing. Secondly, when stacking the layers, the interactions between each layer also need to be carefully managed. For exam-

ple, if a conductive material is required, the layer-to-layer atomic order should be coherent to eliminate any trap states and thus enable the electronic performance. An annealing step to trigger reorganization and crystallization may be required in printing of each layer. Thirdly, with all these steps described above incorporated in the loop, another issue will be the print speed and sample manipulation. If a thousand layers need to be printed and the sample needs to be transferred between machines for each layer, the overall fabrication time would be non-realistic. A solution to this problem may be an integrated printing machine, and meanwhile the printing cycles, which stacks the layers, and the post-treatment, which cleans the sample and ensure property and performance, are separated.

It can be envisioned that in the near future, when 2D layers with no contaminants, high resolution and long-range order are available, fabrication machines will emerge for engineers to design complicated heterostructures and realize unprecedented device performance.

Photolithography

Photolithography has been intensively exploited in the integrated circuit industry. Most of the photolithographic techniques use a mediated way to pattern materials. Photoresist (photopolymerized organics) are first applied homogeneously onto a layer of materials. Then a patterned light source is projected, selectively photopolymerize the exposed area. After rinsing off unreacted photoresist, the remained pattern serves as a blocker to etching. Finally, after etching and following cleaning steps, the materials are successfully patterned.

Different from the mediated way of photolithography, what I described in chapter 2 directly deposit materials in exposed areas without the aid of photoresist. Direct photolithography. Here the materials are directly responsive the light, and there-

fore there is no need of applying photoresist. The working flow of photolithography, when in a direct way, can be largely simplified, because the steps are eliminated including applying photoresist, development of photoresist, etc. By eliminating steps, chances of introducing uncertainties and quality variances are also reduced. Challenges still exist. Since most inorganic materials do not undergo structural change as a respond to light, the direct photolithography techniques still require a organic-inorganic hybrid system, and here it refers to a nanocrystal coated by photoresponsive organic ligands. The organic lignad shells act as a wrap to pack the inorganic materials inside, and the packages within exposed areas will be unraveled and released. How to completely remove the organic part is still a challenge. Channels for the escape of stripped organics have to be created, and driving forces to push the organics through the channel are needed. To work on a fluid interface seems to be one possible solution, because the liquid subphase serves readily as a channel for the organics to dissolve in. However, it has some fatal manipulation problems. Firstly, due to the mobile nature of a liquid platform, it is susceptible to a number of external factors, such as airflow and unsteadiness. Secondly, the contact angle at the interface of the reaction container and liquid subphase will change the shape of liquid surface due to surface tension. To maintain a consistent surface shape profile, the cleaning of reaction container is very strict because any residual of chemicals will alter the contact angle. Thirdly, during the transfer of printed patterns, there will be an inevitable possiblity of distortion. In addition, transfering any printed sample to a substrate, where an ordered structrue is already built, is subject to misalignment of features.

To conclude, photolithography at fluid interface may not be the right direction. Assembly process at fluid interface still possess its merit, which is the ability to build ultrathin layers (down to monolayer of dots). Therefore, a right track may

be fabrication of ultrathin layers at fluid interface and photolithography at solid substrate.

4.3 Outlook

CQDs are intriguing in the application at curved surfaces for its flexibility. Bulk materials are rigid and fragile. Integration of QD with conductive polymers.

4.3.1 Future Works

In this subsection, future projects that can be initiated within relatively a short term will be discussed. Most of the projects are based on techniques and tools developed in chapter 2 & 3.

High Performance Separation Membrane for Li-S Batteries

Coordinate polymers (CPs) are promising candidates for precise separation applications. Compared to polymer membranes, CPs based membranes have size-selective windows precisely defined by coordination chemistry that offer additional separation of mass flow other than diffusion rate difference. Metal-organic-framework (MOF) materials also possess precise micropores, but small size of MOF crystallites, time and cost intensive preparationk, lack of mesoscale pores for effective mass diffusion all impair its application as separation membranes.
Lithium sulfur (Li-S) batteries are composed of a lithium metal anode, a sulfur composite cathode and a separator between the two electrodes. Li-S batteries are

of great research interest due to the high energy density.[33] However, the free migration of polysulfide anions between cathode and anode severely hamper the Coulombic efficiency, leading to a so-called shuttle effect.[11] Therefore, high performance separators are needed to suppress the migration of polysulfides between electrodes while maintain a successful diffusion of electrolytes.

Seletive Impurity Digesting

In biosystems, challenging multitask applications are expected due to the complicated environment. Nanocomposite is a solution since it possess multiple functions by incorporating different materials. These functions include recognition, reaction, repository, etc.

CPs have precisely defined windows such that when a mixture of molecules flows through, only molecules with size smaller than the windows can enter. Therefore, coatings of CPs can prevent large molecules from reaction with the core. To be specific, catalytic cores, such as organic phosphores, metal complexes and quantum dots, when incorporated in CP coating, can selectively catalyze the reaction of small molecules in the system. This nanocomposite may serve as 'nanofactories' to photocatalyze the degradation of small molecule impurities while protect other large valuable molecules such as drugs, proteins and DNAs. This can largely extend the life cycle of separation columns, and thus relieving the consideration of fabrication complexity and implementation cost of these devices.

Porous Superstructure for Heterogeneous Catalysis

With stereolithography and the ability to pattern quantum dot layers, 3D porous superstructure of organic-free semiconductor materials can be created. The poros-

ity can enhance the mass transport and increase effective surface adsorption sites. Therefore, this porous media will be a desired platform for heterogeneous catalysis. Porous photoelectrodes made with mixture of quantum dots can possess multiple heterojunctions with tunable band gap. Therefore, the absorption can be tuned towards visible regions for more efficient solar energy harvesting.[48, 35]

BIBLIOGRAPHY

[1] A Paul Alivisatos. Semiconductor clusters, nanocrystals, and quantum dots. *science*, 271(5251):933–937, 1996.

[2] Nicholas C Anderson, Mark P Hendricks, Joshua J Choi, and Jonathan S Owen. Ligand exchange and the stoichiometry of metal chalcogenide nanocrystals: spectroscopic observation of facile metal-carboxylate displacement and binding. *Journal of the American Chemical Society*, 135(49):18536–18548, 2013.

[3] Daniel M Balazs, Tyler A Dunbar, Detlef-M Smilgies, and Tobias Hanrath. Coupled dynamics of colloidal nanoparticle spreading and self-assembly at a fluid–fluid interface. *Langmuir*, 36(22):6106–6115, 2020.

[4] Daniel M Balazs, Bartosz M Matysiak, Jamo Momand, Artem G Shulga, Maria Ibáñez, Maksym V Kovalenko, Bart J Kooi, and Maria Antonietta Loi. Electron mobility of 24 cm2 v- 1 s- 1 in pbse colloidal-quantum-dot superlattices. *Advanced Materials*, 30(38):1802265, 2018.

[5] Sonwabo E Bambalaza, Henrietta W Langmi, Robert Mokaya, Nicholas M Musyoka, Jianwei Ren, and Lindiwe E Khotseng. Compaction of a zirconium metal–organic framework (uio-66) for high density hydrogen storage applications. *Journal of Materials Chemistry A*, 6(46):23569–23577, 2018.

[6] Clive R Bealing, William J Baumgardner, Joshua J Choi, Tobias Hanrath, and Richard G Hennig. Predicting nanocrystal shape through consideration of surface-ligand interactions. *ACS nano*, 6(3):2118–2127, 2012.

[7] Michael A Boles, Daishun Ling, Taeghwan Hyeon, and Dmitri V Talapin. The surface science of nanocrystals. *Nature materials*, 15(2):141–153, 2016.

[8] Louis E Brus. Electron–electron and electron-hole interactions in small semiconductor crystallites: The size dependence of the lowest excited electronic state. *The Journal of chemical physics*, 80(9):4403–4409, 1984.

[9] Bart Bueken, Niels Van Velthoven, Tom Willhammar, Timothée Stassin, Ivo Stassen, David A Keen, Gino V Baron, Joeri FM Denayer, Rob Ameloot, Sara Bals, et al. Gel-based morphological design of zirconium metal–organic frameworks. *Chemical science*, 8(5):3939–3948, 2017.

[10] Jin Chang and Eric R Waclawik. Colloidal semiconductor nanocrystals: controlled synthesis and surface chemistry in organic media. *RSC Advances*, 4(45):23505–23527, 2014.

[11] Sang-Eun Cheon, Ki-Seok Ko, Ji-Hoon Cho, Sun-Wook Kim, Eog-Yong Chin, and Hee-Tak Kim. Rechargeable lithium sulfur battery: I. structural change of sulfur cathode during discharge and charge. *Journal of the Electrochemical Society*, 150(6):A796, 2003.

[12] Jessica Cimada daSilva, Michelle A Smeaton, Tyler Allan Dunbar, Yuanze Xu, Daniel Mate Balazs, Lena F Kourkoutis, and Tobias Hanrath. Mechanistic insights into superlattice transformation at a single nanocrystal level using nanobeam electron diffraction. *Nano Letters*, 2020.

[13] Nathaniel Corrigan, Jonathan Yeow, Peter Judzewitsch, Jiangtao Xu, and Cyrille Boyer. Seeing the light: advancing materials chemistry through photopolymerization. *Angewandte Chemie International Edition*, 58(16):5170–5189, 2019.

[14] Alexey I Ekimov, Al L Efros, and Alexei A Onushchenko. Quantum size effect in semiconductor microcrystals. *Solid State Communications*, 56(11):921–924, 1985.

[15] Wiel H Evers, Bart Goris, Sara Bals, Marianna Casavola, Joost De Graaf, Rene Van Roij, Marjolein Dijkstra, and Daniel Vanmaekelbergh. Low-dimensional semiconductor superlattices formed by geometric control over nanocrystal attachment. *Nano letters*, 13(6):2317–2323, 2013.

[16] Liang Feng, Kun-Yu Wang, Jeremy Willman, and Hong-Cai Zhou. Hierarchy in metal–organic frameworks. *ACS Central Science*, 6(3):359–367, 2020.

[17] Liang Feng, Shuai Yuan, Liang-Liang Zhang, Kui Tan, Jia-Luo Li, Angelo Kirchon, Ling-Mei Liu, Peng Zhang, Yu Han, Yves J Chabal, et al. Creating hierarchical pores by controlled linker thermolysis in multivariate metal–organic frameworks. *Journal of the American Chemical Society*, 140(6):2363–2372, 2018.

[18] Maw Lin Foo, Ryotaro Matsuda, and Susumu Kitagawa. Functional hybrid porous coordination polymers. *Chemistry of materials*, 26(1):310–322, 2014.

[19] Hiroyasu Furukawa, Felipe Gandara, Yue-Biao Zhang, Juncong Jiang, Wendy L Queen, Matthew R Hudson, and Omar M Yaghi. Water adsorp-

tion in porous metal–organic frameworks and related materials. *Journal of the American Chemical Society*, 136(11):4369–4381, 2014.

[20] Jaco J Geuchies, Carlo Van Overbeek, Wiel H Evers, Bart Goris, Annick De Backer, Anjan P Gantapara, Freddy T Rabouw, Jan Hilhorst, Joep L Peters, Oleg Konovalov, et al. In situ study of the formation mechanism of two-dimensional superlattices from pbse nanocrystals. *Nature materials*, 15(12):1248–1254, 2016.

[21] Junling Guo, Blaise L Tardy, Andrew J Christofferson, Yunlu Dai, Joseph J Richardson, Wei Zhu, Ming Hu, Yi Ju, Jiwei Cui, Raymond R Dagastine, et al. Modular assembly of superstructures from polyphenol-functionalized building blocks. *Nature nanotechnology*, 11(12):1105–1111, 2016.

[22] Yong Hu and Christof M Niemeyer. From dna nanotechnology to material systems engineering. *Advanced Materials*, 31(26):1806294, 2019.

[23] Alexander H Ip, Susanna M Thon, Sjoerd Hoogland, Oleksandr Voznyy, David Zhitomirsky, Ratan Debnath, Larissa Levina, Lisa R Rollny, Graham H Carey, Armin Fischer, et al. Hybrid passivated colloidal quantum dot solids. *Nature nanotechnology*, 7(9):577–582, 2012.

[24] Guan-Young Jeong, Ajay K Singh, Min-Gyu Kim, Ki-Won Gyak, UnJin Ryu, Kyung Min Choi, and Dong-Pyo Kim. Metal-organic framework patterns and membranes with heterogeneous pores for flow-assisted switchable separations. *Nature communications*, 9(1):1–9, 2018.

[25] Cherie R Kagan, Efrat Lifshitz, Edward H Sargent, and Dmitri V Talapin. Building devices from colloidal quantum dots. *Science*, 353(6302), 2016.

[26] Maksym V Kovalenko, Liberato Manna, Andreu Cabot, Zeger Hens, Dmitri V Talapin, Cherie R Kagan, Victor I Klimov, Andrey L Rogach, Peter Reiss, Delia J Milliron, et al. Prospects of nanoscience with nanocrystals, 2015.

[27] Cher Hon Lau, Ravichandar Babarao, and Matthew R Hill. A route to drastic increase of co 2 uptake in zr metal organic framework uio-66. *Chemical Communications*, 49(35):3634–3636, 2013.

[28] Jingang Li, Eric H Hill, Linhan Lin, and Yuebing Zheng. Optical nanoprinting of colloidal particles and functional structures. *ACS nano*, 13(4):3783–3795, 2019.

[29] Peng Li, Justin A Modica, Ashlee J Howarth, Ernesto Vargas, Peyman Z Moghadam, Randall Q Snurr, Milan Mrksich, Joseph T Hupp, and Omar K Farha. Toward design rules for enzyme immobilization in hierarchical mesoporous metal-organic frameworks. *Chem*, 1(1):154–169, 2016.

[30] Guoqiang Liu, Michael Hirtz, Harald Fuchs, and Zijian Zheng. Development of dip-pen nanolithography (dpn) and its derivatives. *Small*, 15(21):1900564, 2019.

[31] Guoqiang Liu, Sarah Hurst Petrosko, Zijian Zheng, and Chad A Mirkin. Evolution of dip-pen nanolithography (dpn): From molecular patterning to materials discovery. *Chemical Reviews*, 2020.

[32] Liping Liu, Zhongbin Zhuang, Ting Xie, Yang-Gang Wang, Jun Li, Qing Peng, and Yadong Li. Shape control of cdse nanocrystals with zinc blende structure. *Journal of the American Chemical Society*, 131(45):16423–16429, 2009.

[33] Arumugam Manthiram, Yongzhu Fu, Sheng-Heng Chung, Chenxi Zu, and Yu-Sheng Su. Rechargeable lithium–sulfur batteries. *Chemical reviews*, 114(23):11751–11787, 2014.

[34] Abdul Khayum Mohammed, Saurabh Usgaonkar, Fayis Kanheerampockil, Suvendu Karak, Arjun Halder, Minakshi Tharkar, Matthew Addicoat, Thalasseril G Ajithkumar, and Rahul Banerjee. Connecting microscopic structures, mesoscale assemblies, and macroscopic architectures in 3d-printed hierarchical porous covalent organic framework foams. *Journal of the American Chemical Society*, 142(18):8252–8261, 2020.

[35] Savio JA Moniz, Stephen A Shevlin, David James Martin, Zheng-Xiao Guo, and Junwang Tang. Visible-light driven heterojunction photocatalysts for water splitting–a critical review. *Energy & Environmental Science*, 8(3):731–759, 2015.

[36] CBea Murray, David J Norris, and Moungi G Bawendi. Synthesis and characterization of nearly monodisperse cde (e= sulfur, selenium, tellurium) semiconductor nanocrystallites. *Journal of the American Chemical Society*, 115(19):8706–8715, 1993.

[37] Christopher B Murray, a CR Kagan, and MG Bawendi. Synthesis and characterization of monodisperse nanocrystals and close-packed nanocrystal assemblies. *Annual review of materials science*, 30(1):545–610, 2000.

[38] Lionel Nicole, Christel Laberty-Robert, Laurence Rozes, and Clément Sanchez. Hybrid materials science: a promised land for the integrative design of multifunctional materials. *Nanoscale*, 6(12):6267–6292, 2014.

[39] Lionel Nicole, Laurence Rozes, and Clément Sanchez. Integrative approaches to hybrid multifunctional materials: from multidisciplinary research to applied technologies. *Advanced Materials*, 22(29):3208–3214, 2010.

[40] Xiaogang Peng, Liberato Manna, Weidong Yang, Juanita Wickham, Erik Scher, Andreas Kadavanich, and A Paul Alivisatos. Shape control of cdse nanocrystals. *Nature*, 404(6773):59–61, 2000.

[41] Katherine R Phillips, Grant T England, Steffi Sunny, Elijah Shirman, Tanya Shirman, Nicolas Vogel, and Joanna Aizenberg. A colloidoscope of colloid-based porous materials and their uses. *Chemical Society Reviews*, 45(2):281–322, 2016.

[42] Laurence Rozes and Clément Sanchez. Titanium oxo-clusters: precursors for a lego-like construction of nanostructured hybrid materials. *Chemical Society Reviews*, 40(2):1006–1030, 2011.

[43] Constanze Schliehe, Beatriz H Juarez, Marie Pelletier, Sebastian Jander, Denis Greshnykh, Mona Nagel, Andreas Meyer, Stephan Foerster, Andreas Kornowski, Christian Klinke, et al. Ultrathin pbs sheets by two-dimensional oriented attachment. *Science*, 329(5991):550–553, 2010.

[44] Yue-xiao Shen, Woochul Song, D Ryan Barden, Tingwei Ren, Chao Lang, Hasin Feroz, Codey B Henderson, Patrick O Saboe, Daniel Tsai, Hengjing Yan, et al. Achieving high permeability and enhanced selectivity for angstrom-scale separations using artificial water channel membranes. *Nature communications*, 9(1):1–11, 2018.

[45] Dmitri V Talapin, Jong-Soo Lee, Maksym V Kovalenko, and Elena V Shevchenko. Prospects of colloidal nanocrystals for electronic and optoelectronic applications. *Chemical reviews*, 110(1):389–458, 2010.

[46] Krunoslav Užarević, Timothy C Wang, Su-Young Moon, Athena M Fidelli, Joseph T Hupp, Omar K Farha, and Tomislav Friščić. Mechanochemical and solvent-free assembly of zirconium-based metal–organic frameworks. *Chemical communications*, 52(10):2133–2136, 2016.

[47] Ben Van de Voorde, Bart Bueken, Joeri Denayer, and Dirk De Vos. Adsorptive

separation on metal–organic frameworks in the liquid phase. *Chemical Society Reviews*, 43(16):5766–5788, 2014.

[48] Gongming Wang, Xunyu Yang, Fang Qian, Jin Z Zhang, and Yat Li. Double-sided cds and cdse quantum dot co-sensitized zno nanowire arrays for photoelectrochemical hydrogen generation. *Nano letters*, 10(3):1088–1092, 2010.

[49] Yuanyuan Wang, Igor Fedin, Hao Zhang, and Dmitri V Talapin. Direct optical lithography of functional inorganic nanomaterials. *Science*, 357(6349):385–388, 2017.

[50] Kevin Whitham and Tobias Hanrath. Formation of epitaxially connected quantum dot solids: nucleation and coherent phase transition. *The Journal of Physical Chemistry Letters*, 8(12):2623–2628, 2017.

[51] Kevin Whitham, Detlef-M Smilgies, and Tobias Hanrath. Entropic, enthalpic, and kinetic aspects of interfacial nanocrystal superlattice assembly and attachment. *Chemistry of Materials*, 30(1):54–63, 2018.

[52] Kevin Whitham, Jun Yang, Benjamin H Savitzky, Lena F Kourkoutis, Frank Wise, and Tobias Hanrath. Charge transport and localization in atomically coherent quantum dot solids. *Nature materials*, 15(5):557–563, 2016.

[53] Xiao-Yu Yang, Li-Hua Chen, Yu Li, Joanna Claire Rooke, Clément Sanchez, and Bao-Lian Su. Hierarchically porous materials: synthesis strategies and structure design. *Chemical Society Reviews*, 46(2):481–558, 2017.

[54] Shuai Yuan, Lanfang Zou, Jun-Sheng Qin, Jialuo Li, Lan Huang, Liang Feng, Xuan Wang, Mathieu Bosch, Ali Alsalme, Tahir Cagin, et al. Construction of hierarchically porous metal–organic frameworks through linker labilization. *Nature communications*, 8(1):1–10, 2017.

[55] Danylo Zherebetskyy, Marcus Scheele, Yingjie Zhang, Noah Bronstein, Christopher Thompson, David Britt, Miquel Salmeron, Paul Alivisatos, and Lin-Wang Wang. Hydroxylation of the surface of pbs nanocrystals passivated with oleic acid. *Science*, 344(6190):1380–1384, 2014.